Human DICER helicase domain recruits PKR and modulates its antiviral activity

Thomas C. Montavon[1,*], Morgane Baldaccini[1,*], Mathieu Lefèvre[1,*], Erika Girardi[1], Béatrice Chane-Woon-Ming[1], Mélanie Messmer[1], Philippe Hammann[2], Johana Chicher[2], Sébastien Pfeffer[1,‡]

[1] Université de Strasbourg, Architecture et Réactivité de l'ARN, Institut de Biologie Moléculaire et Cellulaire du CNRS, 2 allée Konrad Roentgen, 67084 Strasbourg France

[2] Université de Strasbourg, Institut de Biologie Moléculaire et Cellulaire du CNRS, Plateforme Protéomique Strasbourg – Esplanade, 2 allée Konrad Roentgen, 67084 Strasbourg France

*These authors contributed equally

‡ To whom correspondence should be addressed: spfeffer@unistra.fr

Short title: Regulation of PKR by DICER in viral infection

Abstract

The antiviral innate immune response mainly involves type I interferon (IFN) in mammalian cells. The contribution of the RNA silencing machinery remains to be established, but several recent studies indicate that the ribonuclease DICER can generate viral siRNAs in specific conditions. It has also been proposed that type I IFN and RNA silencing could be mutually exclusive antiviral responses. In order to decipher the implication of DICER during infection of human cells with alphaviruses such as the Sindbis virus and Semliki forest virus, we determined its interactome by proteomics analysis. We show that DICER specifically interacts with several double-stranded RNA binding proteins and RNA helicases during viral infection. In particular, proteins such as DHX9, ADAR-1 and the protein kinase RNA-activated (PKR) are enriched with DICER in virus-infected cells. We demonstrate that the helicase domain of DICER is essential for this interaction and that its deletion confers antiviral properties to DICER in an RNAi-independent, PKR-dependent, manner.

Author summary

While RNAi has been recognized as an efficient antiviral defense system in organisms such as plants and insects, its physiological importance in mammals remains to be determined. DICER is an enzyme involved in cleaving long double-stranded RNAs and is essential for RNAi induction. Using mass spectrometry analysis, we determined its interactome in human cells and showed that RNA binding proteins such as PKR are specifically enriched upon infection with the Sindbis virus or the Semliki forest virus. We determined that the N terminal helicase domain of the DICER protein acts as a platform to recruit these factors during infection and that its deletion confers an antiviral activity to DICER.

Introduction

In mammalian cells, the main antiviral defense system involves the activation of a signaling cascade relying on production of type I interferon (IFN I). This pathway depends on the recognition of extrinsic signals or pathogen associated molecular patterns (PAMPs) by dedicated host receptors. Double-stranded (ds) RNA, which can originate from viral replication or convergent transcription, is a very potent PAMP and can be sensed in the cell by various proteins among which a specific class of DExD/H-box helicases called RIG-I-like receptors (RLRs) [1]. RLRs comprise RIG-I, MDA5 and LGP2 and transduce viral infection signals to induce expression of IFN I cytokines that act in autocrine and paracrine fashion. These cytokines then trigger the expression of hundreds of interferon-stimulated genes (ISGs) to stop the virus in its tracks [2]. Among those ISGs, dsRNA-activated protein kinase R (PKR) plays an important role in antiviral defense by blocking cellular and viral translation upon direct binding to long dsRNA [3]. PKR is a serine-threonine kinase that dimerizes and auto-phosphorylates upon activation. It then phosphorylates numerous cellular targets among which the translation initiation factor eIF2α, which results in the inhibition of cap-dependent translation [4]. Accordingly, translation of many RNA viruses, including alphaviruses, is inhibited by PKR [5–7]. PKR is also involved in other cellular pathways including apoptosis, autophagy and cell cycle [3,8].

RNAi is another evolutionary conserved pathway triggered by long dsRNA sensing [9]. One key component in this pathway is the type III ribonuclease DICER, which is also essential for micro (mi)RNA biogenesis [10,11]. These small regulatory RNAs are sequentially produced by the two ribonucleases DROSHA and DICER, before being loaded into an Argonaute (AGO) effector protein in order to regulate their target mRNAs [12]. Whatever its substrate, be it long dsRNA or miRNA precursor, DICER relies on interacting with co-factors to be fully functional. In mammalian cells, the TAR-RNA binding protein (TRBP), a dsRNA binding protein (dsRBP), was shown to play a role in the selection of DICER substrates, its stabilization, strand selection and incorporation into AGO2 [13]. The interaction with TRBP is well characterized and depends on the helicase domain of DICER and the third dsRNA binding domain (dsRBD) of TRBP [14]. Another dsRBP, the protein activator of interferon-induced protein kinase R (PACT), was also described as an important cofactor of DICER. Although its function is not fully understood, PACT seems to also participate in miRNA loading and strand selection [15,16] *via* protein-protein interaction between the DICER helicase domain and the third dsRBD of PACT [17].

76 It is now common knowledge that RNAi is the main antiviral defense system in several
77 phyla such as plants, arthropods and nematodes (reviewed in [18]). However, its exact
78 contribution in the mammalian antiviral response remains unclear [19–21]. Recent studies
79 indicate that a functional antiviral RNAi does exist in mammals in specific cases. A functional
80 antiviral RNAi response was first detected in undifferentiated mouse embryonic stem cells [22]
81 lacking the IFN response, suggesting that these two pathways could be incompatible. Indeed,
82 in mammalian somatic cells deficient for MAVS or IFNAR, two components of the interferon
83 response, an accumulation of DICER-dependent siRNAs derived from exogenous long dsRNA
84 was detected [23]. In addition, the RLR LGP2 was found interacting with both DICER and
85 TRBP, blocking respectively siRNA production and miRNA maturation [24–26]. Moreover,
86 AGO4 was recently shown to be involved in antiviral RNAi against Influenza A virus (IAV),
87 Vesicular stomatitis virus (VSV) and Encephalomyocarditis virus (EMCV) [27]. Finally, viral
88 suppressors of RNAi (VSRs) have been shown to prevent DICER from playing an antiviral role
89 in mammalian cells [28,29]. Nonetheless, several studies reported no detection of viral siRNAs
90 in mammalian somatic cells infected with several viruses [30–32]. In somatic cells, only a
91 helicase-truncated form of human DICER could produce siRNAs from IAV genome [33], but
92 it also turned out that these siRNAs cannot confer an antiviral state [34].
93 Based on these conflicting observations, we decided to study the involvement of DICER
94 during infection of human cells with the Sindbis virus (SINV). SINV is a member of the
95 *Togaviridae* family in the alphavirus genus, which is transmitted by mosquitoes to mammals
96 and can induce arthritogenic as well as encephalitic diseases [35]. It is widely used as a
97 laboratory alphaviruses model as it infects several cell types and replicates to high titers. SINV
98 has a positive stranded RNA genome of about 12 kb, which codes for two polyproteins that
99 give rise to non-structural and structural proteins, including the capsid. Moreover, upon viral
100 replication, a long dsRNA intermediate, which can be sensed by the host antiviral machinery,
101 accumulates. Of note, SINV dsRNA can be cleaved into siRNA in insects as well as in human
102 cells expressing the Drosophila DICER-2 protein [36]. Nonetheless, although human DICER
103 has the potential to interact with the viral RNA duplex, we did not find evidence that SINV
104 dsRNA could be processed into siRNAs in somatic mammalian cells [30,36]. We thus
105 hypothesized that specific proteins could interfere with DICER during SINV infection by direct
106 interaction and limit its accessibility and/or activity. To address this hypothesis, we generated
107 HEK293T cells expressing a tagged version of human DICER that could be
108 immunoprecipitated in mock or SINV-infected cells in order to perform a proteomic analysis
109 of its interactome. Among the proteins co-immunoprecipitated with DICER and that were

110 specifically enriched upon infection, we identified dsRBPs such as ADAR1, DHX9, PACT and
111 PKR. We further validated the direct interaction between DICER and PKR upon SINV
112 infection. We also demonstrated that the interactions of the endogenous DICER with PKR,
113 PACT and DHX9 could also be detected in SINV-infected, but not mock-infected, HCT116
114 cells. We dissected the protein domains necessary for this interaction and we found that DICER
115 helicase domain plays a fundamental role as a recruitment platform for PKR but also for other
116 co-factors. Finally, we also show that expression of a helicase-truncated version of DICER has
117 a negative effect on SINV infection. Importantly, this antiviral phenotype is independent of
118 RNAi, but requires the presence of PKR. Our results indicate that DICER interactome is highly
119 dynamic and directly link components of RNAi and IFN pathways in modulating the cellular
120 response to viral infection.
121

122 ## Results

123

124 **Establishment of a HEK293T cell line expressing FLAG-HA tagged DICER**

125 In order to be able to study the interactome of the human DICER protein during viral infection,
126 we transduced *Dicer* knock-out HEK293T cells (NoDice 2.20) [37] with either a lentiviral
127 construct expressing a FLAG-HA-tagged wild type DICER protein (FHA:DICER WT #4) or a
128 construct without insert as a negative control (FHA:ctrl #1). After monoclonal selection of
129 stably transduced cells, we first characterized one clone of both FHA:DICER WT and of the
130 FHA:ctrl cell lines. We first confirmed that the expression of the tagged version of DICER
131 restored the miRNA biogenesis defect observed in the NoDice cells (Fig. S1A). We then
132 monitored the phenotype of these cells during SINV infection by using as a readout of viral
133 infection the modified version of SINV able to express GFP from a duplicated sub-genomic
134 promoter (SINV-GFP) [38]. At 24 hours post-infection (hpi) and a multiplicity of infection
135 (MOI) of 0.02, the GFP fluorescence observed in FHA:DICER WT #4 cells and HEK293T
136 cells was similar. However, the NoDice FHA:ctrl #1 cells displayed a decrease in GFP signal
137 (Fig. 1A). Western blot analysis of GFP expression confirmed the observations by
138 epifluorescence microscopy, *i.e.* a significantly lower accumulation of GFP in the absence of
139 the DICER protein (Fig. 1B). We therefore wished to confirm the effect of DICER loss on
140 SINV-GFP infection in another NoDice cell line, *i.e.* the NoDice clone 4.25 [39], and in another
141 clone of the NoDice 2.20 FHA:ctrl cells (NoDice FHA:ctrl #2). We observed a similar decrease
142 of SINV-GFP infection in NoDice 2.20 cells and two independent NoDice FHA:ctrl clones

143 compared to HEK293T cells as shown by GFP microscopy (Fig. S1B), by titration of the virus
144 (Fig. S1C) and by western blot analysis (Fig. S1D). However, the independent NoDice 4.25
145 *Dicer* knock-out clone appeared mostly unaffected compared to HEK293T cells in term of GFP
146 accumulation and viral titer (Fig. S1B-D). This suggests that, despite the observed slight effect
147 on SINV-GFP in NoDice 2.20 cells (Fig. 1), DICER proviral effect is not reproductible in an
148 independent clone and therefore could not be generalized.

149 In order to evaluate whether different expression levels of DICER in a NoDice
150 background could rescue the SINV infection phenotype observed in HEK293T cells, we also
151 infected both the FHA:DICER WT polyclonal and an independent FHA:DICER WT clone
152 (FHA:DICER WT #17) with SINV-GFP (Fig. 1A and Fig. 1C-D). We confirmed that the GFP
153 fluorescence observed by microscopy (Fig. 1A), as well as the viral titers and the GFP protein
154 accumulation (Fig. 1C-D) in all tested FHA:DICER lines were comparable to the ones observed
155 in HEK293T cells. Moreover, there was no striking difference in AGO2 expression between
156 the FHA:DICER lines (Fig. 1D).

157 Altogether, these results indicate that the FHA-tagged DICER protein can functionally
158 complement the lack of DICER in terms of miRNA biogenesis (Fig. S1A) and can therefore be
159 used for proteomics studies. Moreover, because we could not observe significant differences in
160 terms of SINV infection (Fig. 1) between the different FHA:DICER clones tested, we decided
161 to select one line, namely FHA:DICER WT#4, for further analysis.

162

163 **Analysis of DICER interactome during SINV infection by mass spectrometry**

164 Our molecular tool being validated, we then focused on determining the interactome of
165 FHA:DICER during SINV infection. We wanted to look at DICER interactome at an early
166 infection time point to isolate cellular factors that could potentially modulate either DICER
167 accessibility or its effect on viral dsRNA. As SINV replicates quickly upon cellular entry, we
168 chose to set up the infection conditions to a duration of 6 hours at an MOI of 2.

169 We performed an anti-HA immunoprecipitation experiment (HA IP) coupled to label-
170 free LC-MS/MS analysis in FHA:DICER WT #4 cells either mock-infected or infected for 6 h
171 at an MOI of 2 with SINV-GFP. In parallel, we performed an anti-MYC immunoprecipitation
172 as a negative control (CTL IP). The experiments were performed in technical triplicate in order
173 to have statistically reproducible data for the differential analysis, which was performed using
174 spectral counts. Prior to the detailed analysis of the results, we verified that there was no
175 confounding factor in the experimentation by performing a Principal Component Analysis

176 (PCA). This allowed us to see that the replicates were very homogenous and that the different
177 samples were well separated based on the conditions.

178 To check the specificity of the HA immunoprecipitation, we first compared the proteins
179 identified in the HA IP with the ones identified in the CTL IP in mock-infected cells.
180 Differential expression analysis allowed us to calculate a fold change and an adjusted p-value
181 for each protein identified and to generate a volcano plot representing the differences between
182 HA and CTL IP samples. Applying a fold change threshold of 2 ((LogFC) > 1), an adjusted p-
183 value threshold of 0.05 and a cutoff of at least 5 spectral counts in the most abundant condition,
184 we identified 258 proteins differentially immunoprecipitated between the two conditions out of
185 1318 proteins (Fig. 2A and Supp. Table 1). Among these, 123 proteins were specifically
186 enriched in the HA IP. The most enriched protein was DICER, followed by its known co-factors
187 TRBP and PACT (also known as PRKRA) [13,17]. We were also able to retrieve AGO2,
188 indicating that the RISC loading complex was immunoprecipitated and that proteins retrieved
189 in our HA IP are specific to DICER immunoprecipitation.

190 We next performed the differential expression analysis of proteins retrieved in the HA
191 IP in SINV-GFP compared to mock-infected cells. Among 1342 proteins, 296 were
192 differentially retrieved between conditions (Fig. 2B and Supp. Table 2). Of these, 184 proteins,
193 including viral ones, were at least 2-fold enriched in SINV-GFP-infected cells. GO-term
194 analysis showed a significant enrichment in RNA binding proteins including double-stranded
195 RNA binding proteins and RNA helicases (Fig. 2C). We then generated a functional protein
196 association network using STRING on the top 100 proteins enriched in SINV-infected
197 compared to mock-infected cells (Fig. 2D). The resulting STRING network confirmed that a
198 limited number of these proteins are known to be interacting with DICER, but that they are all
199 engaged in other complexes (*e.g.* DHX9, DDX18) that could partly explain the presence of
200 some candidates in the mass spectrometry data. In addition, a large number of these proteins
201 are involved in RNA metabolic processes (Fig. 2D, in red), or in their regulation (in blue), while
202 a whole cluster is composed of dsRNA binding proteins (in green). Among the RNA binding
203 proteins retrieved, the top and most specific DICER interactor is the interferon-induced, double-
204 stranded (ds) RNA-activated protein kinase PKR (also known as E2AK2), which is enriched
205 more than 250 times in virus-infected cells (Fig. 2B and E). We were also able to identify the
206 dsRNA-specific adenosine deaminase protein ADAR-1 (also known as DSRAD), as well as
207 PACT, which were enriched 5.9 and 4.2 times respectively in SINV-GFP-infected cells
208 compared to mock-infected cells (Fig. 2B and E). Among the isolated RNA helicases, we
209 identified the ATP-dependent RNA helicase A protein DHX9, which is implicated in *Alu*

210 element-derived dsRNA regulation and in RISC loading [40,41]. In order to verify if the
211 observed interactions were specific to SINV we performed the same experiments with another
212 virus of the *Togaviridae* family, the Semliki forest virus (SFV). In this analysis, we were able
213 to retrieve ADAR-1, DHX9, PACT and PKR, specifically enriched in SFV-infected samples
214 (Fig. S2 and Supp. Tables 3 and 4). These results show that these interactions can be retrieved
215 in *Togaviridae*-infected cells.
216 Taken together, our data indicate that several proteins interacting with DICER in virus-
217 infected cells are involved in dsRNA sensing and/or interferon-induced antiviral response.
218
219 **DICER and PKR interact *in vivo* in the cytoplasm during SINV infection**
220 To validate the LC-MS/MS analysis, we performed a co-immunoprecipitation (co-IP) followed
221 by western blot analysis in FHA:DICER WT #4 cells infected with SINV-GFP at an MOI of 2
222 for 6 h. Whereas TRBP interacted equally well with FHA:DICER in mock and SINV-GFP-
223 infected cells, ADAR-1, PKR, DHX9 and PACT were only retrieved in the HA IP in SINV-
224 infected cells (Fig. 3A). We verified that these interactions could also be observed at a later
225 time post-infection by performing the HA IP in FHA:DICER WT #4 cells infected with SINV-
226 GFP for 24 h at an MOI of 0.02. This indicates that the specific interactions between DICER
227 and ADAR-1, DHX9, PACT or PKR occur at an early stage of the SINV infection and remain
228 stable in time in virus-infected cells (Fig. S3A).
229 In order to verify whether these interactions were mediated by RNA, we performed an
230 anti-HA co-IP experiment on an RNase A/T1 treated total extract from FHA:DICER WT #4
231 cells infected with SINV-GFP at an MOI of 2 for 6h. Since the RNase treatment was performed
232 at relatively low salt concentration (140 mM NaCl), RNase A should cleave dsRNA [42,43]
233 and we should therefore assess both ss and dsRNA-dependency in these conditions. We
234 confirmed the efficiency of the RNase treatment by ethidium bromide staining visualisation of
235 total RNA on an agarose gel (Fig. S3B). TRBP equally interacted with FHA:DICER, with or
236 without RNase treatment, in mock and SINV-GFP-infected cells (Fig. 3B). Instead, the virus-
237 induced interactions between DICER and PKR or PACT upon SINV-GFP infection were
238 almost totally lost in the RNase-treated samples. Upon virus infection, PKR is phosphorylated
239 to be activated and exert its antiviral function [4]. Using an antibody targeting the
240 phosphorylated form of PKR (p-PKR), we looked for p-PKR before and after RNase treatment.
241 The virus-enriched interactions between DICER and p-PKR or DHX9 were completely lost
242 upon RNase treatment. These results therefore indicate that RNA molecules (either single- or

243 double-stranded) facilitate DICER interaction with DHX9, PACT and PKR and its active form,
244 although the complex may also partially interact in an RNA-independent manner.

245 Because of the involvement of PKR in antiviral response [44] and the fact that it shares
246 common co-factors with DICER, namely TRBP and PACT [45,46], we decided to focus our
247 analysis on the DICER-PKR interaction. To confirm the biological relevance of this interaction,
248 we first performed a reverse co-IP to immunoprecipitate the endogenous PKR protein in
249 HEK293T cells infected or not with SINV-GFP. While PACT interacted with PKR both in
250 mock and in SINV-GFP-infected cells as expected (Fig. 3C lower panel), DICER co-
251 immunoprecipitated with the endogenous PKR only in virus-infected cells as previously
252 observed (Fig. 3C upper panel).

253 To further determine whether DICER and PKR could directly interact *in vivo*, we set up
254 a bi-molecular fluorescent complementation assay (BiFC) experiment [47]. To this end, we
255 fused the N- or C-terminal halves of the Venus protein ($^{N\text{-}ter}$Venus or $^{C\text{-}ter}$Venus) to DICER and
256 to PKR but also to TRBP and PACT. Since we showed above that an N-terminally tagged
257 DICER was functional, we fused the Venus fragments at the N-terminal end of DICER. For the
258 other three proteins, we fused the Venus fragments at the N- or C-terminus and selected the
259 best combination. To avoid interaction with the endogenous DICER and PKR proteins, we
260 conducted all BiFC experiments in NoDice/ΔPKR HEK293T cells [33]. In order to control the
261 BiFC experiments, we chose to exploit the well characterized DICER-TRBP interaction, which
262 is known to occur via the DICER DEAD-box helicase domain [14]. We therefore used the wild-
263 type DICER protein as a positive control and a truncated version of DICER protein lacking part
264 of this helicase domain and called DICER N1 [33] as a negative control (Fig. S3C). We first
265 confirmed the expression of the tagged proteins by western blot analysis (Fig. S3D) and then,
266 we tested the interactions between DICER and TRBP or PACT or PKR. We co-transfected the
267 Venus constructs for 24 h and then infected cells with SINV or not for 6 h at a MOI of 2. A
268 comparable fluorescent signal was observed both in mock- and SINV-infected cells when $^{N-}$
269 ^{ter}Venus:DICER was co-transfected with either PACT or TRBP fusion construct (Fig. 3D).
270 Although we initially expected an increase of the Venus fluorescence in SINV-infected cells,
271 overall we observed a similar signal for the DICER-PKR interaction both in mock- and SINV-
272 infected cells, probably due to the fact that both proteins are transiently overexpressed in this
273 experiment. The same holds true for the DICER-PACT interaction that can also be seen both
274 in mock- and SINV-infected cells.

275 As a control and to rule out any aspecific interactions between the different proteins
276 tested, we also monitored the DICER-N1-TRBP interaction by BiFC. As expected, no
277 fluorescent signal was observed in cells co-transfected with $^{N\text{-}ter}$Venus:DICER N1 and
278 TRBP:Venus$^{C\text{-}ter}$ (Fig. S3E), confirming that DICER helicase domain is required for its
279 interaction with TRBP [14] and validating the specificity of the BiFC approach.
280 To further confirm that the absence of PKR did not influence the interactions of TRBP
281 or PACT with DICER, we also performed a BiFC analysis in HEK293T cells. After verifying
282 that in this context as well, fusion proteins were expressed as expected (Fig. S3F), we observed
283 that the results were similar as in NoDiceΔPKR cells (Fig. S3G).
284 To gain more insight into the subcellular localization of these interactions during SINV
285 infection, we performed the BiFC experiments, fixed the cells and observed them under a
286 confocal microscope. We observed a cytoplasmic fluorescent signal for DICER-TRBP and
287 DICER-PACT interactions (Fig. 3E upper and middle panels), which is in agreement with their
288 canonical localization for the maturation of most miRNAs [10,48]. Similarly, co-transfection
289 of DICER and PKR led to a strong Venus signal homogeneously distributed in the cytoplasm
290 (Fig. 3E lower panel).
291 Collectively, these results formally confirm that DICER interacts with several RNA
292 helicases and dsRNA-binding proteins in virus-infected cells, among which PKR, and that for
293 the latter this interaction occurs in the cytoplasm.
294
295 **DICER interactome changes upon SINV infection are not cell-type specific**
296 To further validate our DICER interactome results and generalize them to another biological
297 system, we performed co-IP experiments on the endogenous DICER in a different cell type. To
298 this end, the FLAG-HA-GFP tag was knocked into (KI) the *Dicer* locus in human colon
299 carcinoma cells (HCT116) by CRISPR-Cas9-mediated homologous recombination (Fig. S4A-
300 C). A guide RNA (gRNA) targeting the region corresponding to Dicer ATG and a DNA
301 template for homologous recombination bearing the FLAG-HA-GFP sequence surrounded by
302 the upstream and downstream arms of Dicer were used to generate the resulting cell line
303 referred to as HCT116 KI-DICER cells. The expected insertion of the tag in one of the two
304 Dicer allele was assessed by PCR amplification and Sanger sequencing (Fig. S4A-C). In
305 agreement, we could detect two bands for DICER protein by western blot in the HCT116 KI-
306 DICER cells, which confirmed that this cell line is heterozygous (Fig. 4A).
307 We additionally verified the expression of specific DICER-interacting proteins, such as
308 AGO2, PKR or TRBP, in HCT116 KI-DICER cells compared to the parental HCT116 cells

309 and to HEK293T cells (Fig. 4A). We also measured the production of mature miRNAs, such
310 as miR-16, by northern blot analysis and confirmed that miRNA expression is maintained in
311 HCT116 KI-DICER cells (Fig. 4B). Of note, the GFP inserted at the *Dicer* locus could not be
312 detected by epifluorescence microscopy in the HCT116 KI-DICER cells, which probably
313 reflects the low abundance of the DICER protein.

314 We then determined whether SINV-GFP infection was comparable in HCT116 cells and
315 HEK293T cells. We infected HCT116, HCT116 KI-DICER and HEK293T cells with SINV-
316 GFP at three different MOI (0.02, 0.1 and 1) and measured GFP fluorescence by microscopy at
317 24 hpi (Fig. 4C). Both HCT116 and HCT116 KI-DICER cells expressed GFP upon infection
318 with SINV-GFP, although with a lower intensity than HEK293T cells. We also verified by
319 western blot analysis the accumulation of GFP and the phosphorylation of both PKR and eIF2α
320 upon SINV-GFP infection of HCT116 KI-DICER and HEK293T cells (Fig. S4D) and chose as
321 optimal SINV-GFP condition of infection in HCT116 KI-DICER cells the MOI of 0.1 for 24h.

322 To validate the DICER interactions observed in HEK293T FHA:DICER cells, we then
323 performed anti-HA co-IP experiments followed by western blot analysis in HCT116 KI-DICER
324 cells infected or not with SINV-GFP. We successfully retrieved TRBP interacting with DICER
325 in both mock and infected cells, whereas DHX9, PKR (phosphorylated or not) and PACT were
326 only retrieved in the HA IP in infected cells (Fig. 4D). These results not only confirm that the
327 endogenous DICER specifically interacts with DHX9, PACT and PKR upon SINV infection,
328 but also that these interactions are not restricted to one specific cell type.

329

330 **The helicase domain of DICER is required for its interaction with PKR**

331 Even though DICER and PKR are likely brought together by RNA, specific protein domains
332 might be involved in stabilizing the complex. Therefore, we next determined the domain of
333 DICER required for its interaction with PKR. Since its helicase domain was previously shown
334 to be involved in the interaction with TRBP and PACT [14,17], we speculated that it could also
335 be implicated in binding PKR. To test this hypothesis, we cloned several versions of DICER
336 proteins wholly or partly deleted of the helicase domain (Fig. 5A DICER N1 and N3). In
337 addition, we also cloned the helicase domain alone (Fig. 5A DICER Hel.) and a DICER variant
338 deleted of its C-terminal dsRNA binding domain (Fig. 5A DICER ΔdsRBD) since this domain
339 could also be involved in protein-protein interaction [49,50]. We then transfected the different
340 versions of DICER WT and the deletion mutant constructs in NoDice cells. In mock and SINV-
341 GFP infected cells, whole cell extracts were subjected to anti-HA and anti-MYC (CTL) IP.

342 TRBP was retrieved in both conditions with DICER WT, Hel. and ΔdsRBD (Fig. 5B and 5C).
343 In mock cells, PACT and PKR were only found weakly interacting with DICER WT (Fig. 5B).
344 In SINV-infected cells, we observed that similar to TRBP and to a lesser extent PACT, N1 and
345 N3 mutations strongly reduced the binding of DICER with PKR (Fig. 5C lanes 2-3 and 7-8).
346 Importantly, we also noted that the helicase domain alone could bind PKR, TRBP and PACT
347 (Fig. 5C lanes 4 and 9). Moreover, the deletion of the dsRNA binding domain of DICER did
348 not affect its interaction with TRBP, PACT and PKR (Fig. 5C lanes 5 and 10). We also looked
349 for p-PKR in our co-IP (Fig. 5C panel p-PKR). We noticed that only WT DICER and its
350 helicase domain were able to interact with p-PKR (Fig. 5C lanes 1&6 and 4&9). The fact that
351 DICER ΔdsRBD did not interact with p-PKR (Fig. 5C lanes 5&10) is striking but could indicate
352 that the phosphorylation of PKR may induce conformation changes preventing its interaction
353 with some domains of DICER. These results reveal that, like for TRBP and PACT, the helicase
354 domain of DICER is required for DICER-PKR/p-PKR interaction during SINV infection.

355 In order to confirm these co-IP experiments, we next decided to perform BiFC
356 experiments using the same conditions as previously. In both mock and SINV-infected cells,
357 only the combinations of DICER WT-PKR and DICER ΔdsRBD-PKR showed a strong Venus
358 signal, while neither DICER N1 nor N3 constructs revealed an interaction with PKR (Fig. 5D).
359 In contrast, the DICER Hel. construct did not seem to interact with PKR in mock-infected cells
360 but appeared to do so in SINV-infected cells as a faint Venus signal could be observed. These
361 results therefore confirmed the co-IP observations for the DICER-PKR interaction. In addition,
362 we also performed a BiFC experiment using the different DICER constructs with TRBP or
363 PACT. Altogether, the BiFC results mostly fitted with the co-IP experiment for the DICER-
364 TRBP (Fig. S5A) and DICER-PACT (Fig. S5B) interactions. TRBP indeed did not seem to
365 interact with the DICER N1 and only slightly with the DICER N3. However, PACT interaction
366 was lost with DICER N1, but not with DICER N3 in mock- and SINV-infected cells (Fig. S5B
367 third panel). This result may be explained by the fact that DICER interacts with PACT *via* the
368 helicase and DUF domains, whereas only the DICER helicase domain is required for its
369 interaction with TRBP [14,17]. In agreement, the Venus signal observed between the DICER
370 Hel. and PACT seemed weaker than the one we observed with TRBP (Fig. S5A and B fourth
371 panels).

372 Taken together these results indicate that DICER interacts with both PKR and its
373 phosphorylated form during SINV infection, and that this interaction requires the helicase
374 domain of DICER.

375 **Functional importance of DICER helicase domain during SINV infection**

376 We then sought to study the functional role of DICER-PKR interaction during viral infection.
377 For this purpose, we decided to use DICER helicase deletion mutants to study SINV infection.
378 To do so, we first generated NoDice HEK293T cells stably expressing FHA-tagged DICER N1
379 (FHA:DICER N1) by lentiviral transduction. As for the FHA:DICER WT cell line, we first
380 selected a clone expressing the tagged DICER N1 at a level similar level to the endogenous
381 DICER protein in HEK293T cells (Fig. 6A). DICER N1 protein has been shown to still be able
382 to produce miRNAs [33]. We thus verified by northern blot analysis that DICER N1 is indeed
383 able to process miRNAs similarly to WT DICER in HEK 293T and FHA:DICER cells, thereby
384 validating the functionality of the tagged protein (Fig. 6B). We next infected HEK293T,
385 FHA:DICER WT #4 and FHA:DICER N1 #6 cells with SINV-GFP and measured virus
386 accumulation by assessing GFP expression by microscopy analysis. Interestingly, the GFP
387 protein level was drastically reduced in FHA:DICER N1 #6 cells compared to FHA:DICER
388 WT #4 and HEK293T cells (Fig. 6C). Encouraged by this observation, we decided to infect
389 with SINV-GFP additional DICER deletion mutants, namely N3 and Hel. We generated stable
390 cell lines for these various mutants by lentiviral transduction in the NoDice 2.20 background
391 and infected those cells with SINV-GFP at an MOI of 0.02 for 24h. We verified by western
392 blot analysis that all selected DICER mutant clones, namely N1 #6, N3 #2.13 and Hel. #2.6,
393 expressed the tagged protein at the expected size and at levels mostly similar to the
394 FHA:DICER WT #4 line (Fig. 6D, first two panels). We also verified the DICER mutants
395 contribution to the endogenous miRNA biogenesis by performing a northern blot analysis on
396 miR-16 accumulation (Fig. S6A).

397 We additionally verified the impact of these DICER mutants on SINV-GFP infection
398 by measuring the GFP intensity of fluorescence by microscopy (Fig. S6B). Our results indicated
399 that GFP accumulation is similar in HEK293T, NoDice 2.20, FHA:DICER WT, Hel. and ctrl
400 cells. However, almost no fluorescence was detected in FHA:DICER N1 #6 and N3 #2.13 cells
401 compared to HEK293T cells (Fig. S6B). The reduction of virus-encoded GFP accumulation
402 and viral production were confirmed by western blot (Fig. 6D) and by plaque assay,
403 respectively (Fig. 6E).

404 Altogether, these results therefore indicate that expressing a helicase truncated
405 version of DICER, which is unable to interact with PKR, appears to confer an antiviral
406 phenotype to SINV infection.

407

408 **The antiviral phenotype of the helicase-truncated DICER mutants is independent of**
409 **AGO2**
410 We finally carried out a functional analysis of the helicase-domain-truncated DICER N1 and
411 N3 mutants to investigate the mechanism of the antiviral phenotype. First, to investigate a
412 potential implication of the RNAi pathway, we performed a knock-down of the AGO2 protein
413 prior to the infection of NoDice cells expressing either WT, N1 or N3 FHA:DICER. AGO2 is
414 the main effector protein in RNA silencing pathways [51] and has been previously shown to be
415 a crucial antiviral RNAi factor against Influenza A virus in mouse embryonic fibroblasts
416 (MEFs) [52]. We transfected either control siRNAs, or siRNAs targeting AGO2 for 48h in
417 NoDice cells stably expressing either an empty vector (FHA:ctrl #2) or WT, N1 or N3
418 FHA:DICER constructs. Cells were then infected with SINV-GFP at an MOI of 0.02 for 24h,
419 and virus accumulation was first assessed by looking at GFP expression by microscopy analysis
420 (Fig. 7A). In all cell lines, no major difference in GFP fluorescence could be observed when
421 comparing cells transfected with the control siRNA or AGO2-specific siRNAs. We verified the
422 knock-down efficiency by western blot analysis and confirmed the microscopy observation by
423 measuring GFP protein accumulation (Fig. 7B). Finally, we measured virus accumulation by
424 plaque assay, and we observed that the antiviral phenotype was clearly visible in FHA:DICER
425 N1 #6 and FHA:DICER N3 #2.13 cell lines but was not complemented upon AGO2 knock-
426 down (Fig. 7C).
427 Altogether, these results indicate that the antiviral phenotype against SINV observed in
428 cells expressing helicase-truncated mutant DICER proteins does not depend on the presence of
429 AGO2, thereby ruling out an involvement of RNAi.
430
431 **The antiviral phenotype due to the DICER helicase-domain deletion requires PKR**
432 In order to determine the functional role of the PKR-DICER interaction in the antiviral response
433 to SINV, we generated NoDiceΔPKR cells stably expressing either the full length FHA:DICER
434 WT or the helicase deletion mutants FHA:DICER N1 or N3, or the empty vector as a control
435 (FHA:ctrl) by lentiviral transduction. After monoclonal selection of each cell line, we infected
436 them with SINV-GFP at an MOI of 0.02 and assessed virus accumulation by looking at GFP
437 fluorescence by microscopy analysis (Fig. 8A). As expected, an increase in GFP fluorescence
438 was observed in NoDiceΔPKR FHA:ctrl cells compared to HEK293T cells at 24 hpi. In contrast
439 we could not observe any difference in GFP fluorescence between NoDiceΔPKR FHA:ctr cells
440 and those expressing FHA:DICER WT, FHA:DICER N1 or N3 proteins. To verify whether any
441 significant difference in terms of virus accumulation could be observed in NoDiceΔPKR cells

442 expressing WT or helicase truncated DICER proteins, we measured GFP protein levels by
443 western blot analysis (Fig. 8B) and virus production by plaque assay (Fig. 8C). As opposed to
444 the observations done in cells NoDice cells expressing PKR (Fig. 6), both GFP accumulation
445 and viral titers remained unchanged between NoDiceΔPKR FHA:ctrl cells and those expressing
446 FHA:DICER WT, N1 or N3 constructs. Taken together, these results demonstrate that the
447 antiviral phenotype of helicase-truncated DICER mutants depends on the presence of PKR.
448 Therefore, our data suggest that the helicase domain of DICER sequesters PKR and when this
449 interaction is lost, the antiviral effect of PKR is exacerbated, thereby explaining the phenotype
450 observed in cells expressing helicase-truncated DICER mutants.
451

452 **Discussion**

453 The role of DICER in antiviral defense in human cells remains a topic of intense discussion
454 [21,22,53,54]. In particular there have been contradictory reports regarding its capacity to
455 produce siRNAs from viral RNAs [31,37,55,56]. These observations could be due to the fact
456 that several mammalian viruses potentially encode VSR proteins, thereby masking the effect of
457 RNAi [22,28,29,52,57]. Another putative but non-exclusive explanation could be that there is
458 a mutual regulation of type I IFN and RNAi pathways [58,59]. Thus, it has already been shown
459 that PACT can regulate MDA5 and RIG-I during virus infection and therefore the induction of
460 type I IFN response [60,61]. To date, it is not clear whether the activity of the DICER protein
461 as well could be regulated by potential interactors, or inversely whether it could itself modulate
462 the activity of proteins involved in the IFN pathway. To answer this question, we determined
463 the changes in the interactome of human DICER upon SINV and SFV infection. This analysis
464 allowed us to reveal that a lot of proteins associating with DICER during viral infection are
465 dsRNA-binding proteins and RNA helicases. A number of these proteins are known to be
466 involved in antiviral defense pathways, thereby indicating the possible formation of one or
467 several complexes between DICER and these proteins, which are very likely brought together
468 by the accumulation of dsRNA during virus infection.

469 Among these proteins, we chose to focus on the well-known ISG PKR, which is
470 involved in many cellular pathways such as apoptosis, cellular differentiation, development and
471 antiviral defense [4,8,62,63]. PKR is one of the main actors of the Integrative Stress Response
472 (ISR) in human cells, and its activation or inhibition needs to be tightly regulated in order to
473 have a properly balanced response to stress. Our results indicate that DICER interacts via its
474 helicase domain with PKR in the cytoplasm during SINV infection. The helicase domain of

475 DICER, which is also required for its interaction with TRBP and PACT, belongs to the helicase
476 superfamily 2, which is also found in RLRs such as RIG-I, MDA5 or LGP2 [64,65]. These
477 proteins act as sensors of viral infection and through the activation of proteins such as MAVS,
478 mediate the induction of type I IFN pathway [65]. We hypothesize that even though the human
479 DICER helicase has evolved mainly to act in miRNA/siRNA pathway, it still retained the
480 capacity to act as an RLR. However, as opposed to RIG-I and MDA5, our data suggest that
481 DICER would act more as an inhibitor rather than inducer of the immune response. Therefore,
482 we propose that this domain serves as a platform for the recruitment of different proteins to
483 diversify the function of DICER.

484 One such regulatory effect appears to be on the antiviral activity of PKR, as cells
485 expressing a truncated form of DICER unable to interact with PKR become resistant to SINV
486 infection. This is in agreement with previous observations that ectopic expression of the
487 *Drosophila* DICER2 protein in human cells perturbs IFN signaling pathways and antagonizes
488 PKR-mediated antiviral immunity [36]. Although the precise molecular mechanism involved
489 will require further work to be fully deciphered, it seems that the two proteins are likely brought
490 together *via* their interaction with RNA, most probably of viral origin. Indeed, we showed that
491 the co-IP interaction was partially RNase sensitive. However, we confirmed that the interaction
492 is not artificially created during the co-immunoprecipitation procedure, since we could show
493 that DICER and PKR interact in BiFC assay, a technique that favors the detection of direct
494 interactions [47]. Most of the time, the inhibition of PKR activity relies on its inhibition to bind
495 to dsRNA or to auto-phosphorylate. For example, the human tRNA-dihydrouridine synthase 2
496 (hDus2) binds the first dsRBD of PKR and prevents its activation [66]. TRBP binds dsRNAs
497 but also PKR directly hindering its dimerization. In normal condition, TRBP is also associated
498 with PACT thus preventing PKR activation by PACT [67–70]. Since we showed that DICER
499 can bind the activated phospho-PKR, we hypothesize that this interaction does not result in the
500 inhibition of PKR autophosphorylation. In fact, in condition of infection with a high virus dose,
501 we showed that phospho-PKR levels are similar in cells expressing DICER WT or helicase
502 deletion mutants N1 and N3, but the activated PKR does not associate with these truncated
503 versions of DICER. Therefore, one possibility could be that DICER interaction with PKR
504 prevents the latter from acting upon some of its targets, which remain to be identified, to fine-
505 tune the antiviral response.

506 As of now, we cannot formally rule out that the effect of DICER on PKR is mediated
507 by other proteins. TRBP and PACT have been shown to regulate PKR activity, the former
508 normally acting as a repressor and the latter as an activator [46,68,70]. Interestingly, in

509 lymphocytic Jurkat cells infected by HIV-1, PACT can also act as a repressor of PKR [71]. It
510 is thus tempting to speculate that these two proteins participate in the formation of the DICER-
511 PKR complex. However, our results show that this may not necessarily be the case. Indeed, in
512 the BiFC experiment, the DICER N3 mutant still interacted with PACT but not with PKR
513 indicating that PACT binding is not sufficient to confer the association with PKR.

514 Besides PKR, other proteins were specifically enriched upon viral infection in the
515 DICER IP. These are also interesting candidates to explain the putative regulatory role of
516 DICER. Among these proteins, DHX9 and ADAR-1 are especially intriguing. DHX9, also
517 known as RNA helicase A (RHA), associates with RISC, helping the RISC loading [41].
518 Moreover, DHX9 is directly involved in removing toxic dsRNAs from the cell to prevent their
519 processing by DICER [40]. It has also been implicated in HIV-1 replication and knockdown of
520 DXH9 leads to the production of less infectious HIV-1 virions [72–74]. Finally, DXH9 interacts
521 with and is phosphorylated by PKR in MEFs. This phosphorylation precludes the association
522 of DHX9 with RNA, thus inhibiting its proviral effect [75]. In light of these observations and
523 ours, we can speculate that the inhibitory effect of DICER on PKR activity could also be linked
524 to DHX9 phosphorylation. ADAR-1 is one of the well-known RNA-editing factors [76].
525 ADAR-1 is linked to both miRNA biogenesis [77–79] and virus infection. Indeed, ADAR-1
526 has an antiviral effect against Influenza virus, but most of the time, its depletion leads to a
527 decrease of the viral titer, as was reported for VSV or HIV-1 [80,81]. It has been shown that
528 ADAR-1 and PKR interact directly during HIV-1 infection. This interaction triggers the
529 inhibition of PKR activation, and thus a reduction of eIF2α phosphorylation leading to an
530 increase of virus replication [5,82]. Interestingly, over-expression of ADAR-1 enhances
531 drastically the replication of the alphaviruses Chikungunya virus (CHIKV), and Venezuelan
532 equine encephalitis virus (VEEV) most likely by interfering with the IFN induction [83].

533 One hypothesis to explain the virus resistance phenotype of the DICER N1 and N3 cell
534 lines could be an increased processivity of these truncated proteins on long dsRNA substrates
535 [33], which would render DICER RNAi proficient. However, our results are not in favor of this
536 hypothesis, since we show that knocking-down AGO2 does not allow to make cells expressing
537 DICER N1 or N3 more sensitive to SINV infection. AGO2 being the only slicer-proficient
538 Argonaute protein expressed at physiological levels in HEK293T cells, we can confidently
539 conclude that the observed phenotype is RNAi-independent.

540 Finally, we demonstrated that the phenotype of helicase-truncated DICER isoforms
541 depends on PKR expression, because it was completely lost in PKR knockout cell lines. We

542 therefore propose that, at least during infection with SINV, DICER prevents PKR to be fully
543 active by interacting with and potentially sequestrating it. Deciphering the exact molecular
544 mechanism at play will require additional studies in order to get the full picture. Nevertheless,
545 by assessing the interactome of DICER during SINV infection, we have unveiled a new, PKR-
546 dependent, role for the helicase domain of DICER in regulating the cellular response to viral
547 infection.
548

549 ## Material and methods

550 **Plasmids, cloning and mutagenesis**

551 Plasmids used for BiFC experiments were a gift from Dr. Oliver Vugrek from the Ruđer
552 Bošković Institute and described in [47]. The cDNAs of TRBP, PACT and PKR were
553 respectively amplified from (pcDNA-TRBP Addgene #15666) [16], (pcDNA-PACT Addgene
554 #15667) [16], (pSB819-PKR-hum Addgene #20030) [84], and cloned into the four pBiFC
555 vectors by Gateway recombination. DICER N1, N3 Hel. and ΔdsRBD were generated by PCR
556 mutagenesis from pDONR-DICER described in [36] and cloned into the four pBiFC and
557 pDEST-FHA vectors by Gateway recombination. plenti6 FHA-V5 vector was modified from
558 plenti6-V5 gateway vector (Thermo Fisher scientific V49610) by Gibson cloning. DICER WT,
559 N1, N3 and Hel. from pDONR plasmids were cloned into plenti6 FHA-V5 by Gateway
560 recombination. All primers used are listed in Supp. Table 5.
561

562 **Cell lines**

563 HEK293T, HEK293T/NoDice (2.20 and 4.25), and HEK293T/NoDiceΔPKR cell lines were a
564 gift from Pr. Bryan Cullen and described in [33,39]. HCT116 cell line was a gift from Dr.
565 Christian Gaiddon.
566

567 **Generation of Flag-HA-GFP-DICER knock-in cell line by CRISPR/Cas9**

568 To generate the knock-in cell line, the sequence of Flag-HA-GFP was amplified by PCR from
569 the Flag-HA-GFP plasmid [85]. DNA sequences corresponding to 1 Kb upstream (left
570 homology arm) and downstream (right homology arm) the starting codon (ATG) of DICER
571 gene were amplified from HCT116 cell genomic DNA using primer pairs listed in Supp. Table
572 5. The three PCR products were gel-purified and cloned into a linearized pUC19 by In-fusion
573 cloning (Clontech) to obtain the template for homologous recombination (LarmDICER-
574 FlagHAGFP-RarmDICER).

575 Design of the guide RNA targeting the region between Dicer 5'-UTR and its first coding exon
576 for CRISPR/Cas9 mediated knock-in was carried out using the CRISPOR Design Tool [86].
577 Annealed oligonucleotide corresponding to the gRNA (Supp. Table 5) were cloned into the
578 vector pX459 (Addgene #48139) which also encodes *S. pyogenes* Cas9 with 2A-Puro.
579 The sequence of the donor plasmid was additionally mutagenized to disrupt the PAM sequence
580 of the right homology arm to avoid its cleavage by the gRNA.
581 To obtain the knock-in (KI) cell line, 5 x 10^5 HCT116 cells were seeded in a 6 well plate with
582 Dulbecco's modified Eagle medium (DMEM, Gibco®, Life Technologies) supplemented with
583 10% fetal bovine serum (FBS, Clontech) in a humidified atmosphere of 5% CO_2 at 37°C and
584 transfected after 24 hours with the pX459-gRNADicerNterm-Cas9-2A-Puro plasmid and the
585 Leftarm-FlagHAGFP-RightarmDICER donor plasmids at the ratio of 1 to 1 (6 micrograms
586 plasmids in total) using Lipofectamine 2000 according to the manufacturer instructions. 24
587 hours later, puromycin (1mg/mL) was added to the cells to increase the KI efficiency and
588 genomic DNA was isolated from individual colonies few days later.
589 The presence of the Flag-HA-GFP tag in frame with hDICER coding sequence was confirmed
590 by sequencing PCR amplicon from KI cell gDNA. Expression of Flag-HA-GFP N-terminal
591 tagged Dicer protein in the KI cells was confirmed by western blot.
592
593 **Cell culture and transfection**
594 Cells were maintained in Dulbecco's modified Eagle medium (DMEM, Gibco®, Life
595 Technologies) supplemented with 10% fetal bovine serum (FBS, Clontech) in a humidified
596 atmosphere of 5% CO_2 at 37°C. Transfection was performed using Lipofectamine 2000
597 (Invitrogen, ThermoFisher Scientific) according to the manufacturer's instructions.
598
599 **Lentivirus production and generation of stable cell lines**
600 The lentiviral supernatant from single transfer vector was produced by transfecting HEK293T
601 cells (ATCC® CRL-3216™) with 20 µg of the transfer vector, 15 µg of pMDLg/p RRE and 10
602 µg of pRSV-Rev packaging plasmids (Addgene #12251 and Addgene #12253) and the pVSV
603 envelope plasmid (Addgene #8454) using Lipofectamine 2000 (Invitrogen, ThermoFisher
604 Scientific) reagent according to the manufacturer's protocol. Standard DMEM (Gibco®, Life
605 Technologies) medium supplemented with 10% Fetal bovine serum (FBS, Gibco®, Life
606 Technologies) and 100 U/mL of penicillin-Streptomycin (Gibco®, Life Technologies) was
607 used for growing HEK293T cells and for lentivirus production. One 10 cm plate of HEK293T

608 cells at 70-80% confluency was used for the transfection. The medium was replaced 8 hours
609 post-transfection. After 48 hours the medium containing viral particles was collected and
610 filtered through a 0.45μm PES filter. The supernatant was directly used for transfection or
611 stored at -80°C. A 6 well plate of HEK293T/NoDice or HEK293T/NoDiceΔPKR cells at 80%
612 confluency was transduced using 600 μL of lentiviral supernatant either expressing
613 FHA:DICER, N1, N3, Hel. or empty vector, supplemented with 4 ug/mL polybrene (Sigma)
614 for 6 hours. The transduction media was then changed with fresh DMEM for 24 hours and the
615 resistant cell clones were selected for about 6 weeks with blasticidin (15 µg/mL for NoDice or
616 10 μg/mL for NoDiceΔPKR) and subsequently maintained under blasticidin selection.
617
618 **Viral stocks, virus infection**
619 Viral stocks of SINV or SINV-GFP were produced as described in [36]. Cells were infected
620 with SINV or SINV-GFP at an MOI of 0.02, 0.1, 1 or 2 and samples were collected at different
621 time points as indicated in the figure legends.
622
623 **Analysis of viral titer by plaque assay**
624 Vero R cells were seeded in 96-well plates format and were infected with 10-fold serial
625 dilutions infection supernatants for 1 hour. Afterwards, the inoculum was removed, and cells
626 were cultured in 2.5% carboxymethyl cellulose for 72 hours at 37°C in a humidified atmosphere
627 of 5% CO_2. Plaques were counted manually under the microscope and viral titer was calculated
628 according to the formula: *PFU/mL = #plaques/ (Dilution*Volume of inoculum)*
629
630 **Western blot analysis**
631 Proteins were extracted from cells and homogenized in 350 µL of lysis buffer (50 mM Tris-
632 HCl pH 7.5, 150 mM NaCl, 5 mM EDTA, 1% Triton X-100, 0.5% SDS and Protease Inhibitor
633 Cocktail (complete Mini; Sigma Aldrich)). Proteins were quantified by the Bradford method
634 and 20 to 30 µg of total protein extract were loaded on 4-20% Mini-PROTEAN® TGX™
635 Precast Gels (Bio-Rad). After transfer onto nitrocellulose membrane, equal loading was verified
636 by Ponceau staining. For PVDF membrane, equal loading was verified by Coomassie staining
637 after transfer and blotting. Membranes were blocked in 5% milk and probed with the following
638 antibodies: anti-hDicer (1:500, F10 Santa Cruz sc-136979) and anti-hDicer (1:1000, A301-
639 937A Bethyl), anti-TRBP (1:500, D-5 Santa Cruz sc-514124), anti-PKR (1:2500, Abcam
640 ab32506), anti-PACT (1:500, Abcam, ab75749), anti-HA (1:10000, Sigma, H9658), anti-
641 DHX9 (1:500, Abcam ab26271), anti-p-eIF2a (1:1000, Ser-52 Santa Cruz sc-601670), anti-

642 hADAR-1 (1:500 Santa Cruz sc-271854) anti-p-PKR (1:1000 Abcam ab81303) anti-GFP
643 (1:10000, Roche 11814460001) and anti-Tubulin (1:10000, Sigma T6557). Detection was
644 performed using Chemiluminescent Substrate (Pierce, ThermoFisher Scientific) and visualized
645 on a Fusion FX imaging system (Vilber).
646
647 **RNA extraction and northern blot analysis**
648 Total RNA was extracted using Tri-Reagent Solution (Fisher Scientific; MRC, Inc) according
649 to the manufacturer's instructions. Northern blotting was performed on 10 μg of total RNA.
650 RNA was resolved on a 12% urea-acrylamide gel, transferred onto Hybond-NX membrane (GE
651 Healthcare). RNAs were then chemically cross-linked to the membrane during 90 min at 65°C
652 using 1-ethyl-3-[3-dimethylaminopropyl]carbodiimide hydrochloride (EDC) (Sigma Aldrich).
653 Membranes were prehybridized for 30 min in PerfectHyb™ plus (Sigma Aldrich) at 50°C.
654 Probes consisting of oligodeoxyribonucleotides (see Supplementary Table 2) were 5′-end
655 labeled using T4 polynucleotide kinase (ThermoFisher Scientific) with 25 μCi of [γ-32P]dATP.
656 The labeled probe was hybridized to the blot overnight at 50°C. The blot was then washed twice
657 at 50°C for 20 min (5× SSC/0.1% SDS), followed by an additional wash (1× SSC/0.1% SDS)
658 for 5 min. Northern blots were exposed to phosphorimager plates and scanned using a
659 Bioimager FLA-7000 (Fuji).
660
661 **Immunoprecipitation**
662 Immunoprecipitation experiments were carried out either on tagged proteins or on endogenous
663 proteins.
664 *Tagged proteins*: Cells were harvested, washed twice with ice-cold 1× PBS (Gibco®, Life
665 Technologies), and resuspended in 550 μL of lysis buffer (50 mM Tris-HCl pH 7.5, 140 mM
666 NaCl, 1.5 mM $MgCl_2$, 0.1% NP-40), supplemented with Complete-EDTA-free Protease
667 Inhibitor Cocktail (complete Mini; Sigma Aldrich). Cells were lysed by 30 min incubation on
668 ice and debris were removed by 15 min centrifugation at 2000 g and 4°C. An aliquot of the
669 cleared lysates (50 μL) was kept aside as protein Input. Samples were divided into equal parts
670 (250 μL each) and incubated with 15 μL of magnetic microparticles coated with monoclonal
671 HA or MYC antibodies (MACS purification system, Miltenyi Biotech) at 4°C for 1 hour under
672 rotation (10 rpm). Samples were passed through *μ* Columns (MACS purification system,
673 Miltenyi Biotech). The *μ* Columns were then washed 3 times with 200 μL of lysis buffer and 1
674 time with 100 μL of washing buffer (20 mM Tris-HCl pH 7.5). To elute the immunoprecipitated

675 proteins, 95°C pre-warmed 2x Western blot loading buffer (10% glycerol, 4% SDS, 62.5 mM
676 Tris-HCl pH 6.8, 5% (v/v) 2-β-mercaptoethanol, Bromophenol Blue) was passed through the
677 μ Columns. Proteins were analyzed by western blotting or by mass spectrometry.
678 *Endogenous proteins*: mock or SINV-GFP-infected HEK293T cells (MOI of 2) were lysed 6
679 hours post-infection using immunoprecipitation buffer (50mM tris-HCl [pH 7.5], 150mM
680 NaCl, 5mM EDTA, 0.05% SDS, 1% triton) supplemented with Complete-EDTA-free Protease
681 Inhibitor Cocktail (complete Mini; Sigma Aldrich). Lysates were treated for 20 min at 37°C
682 with 1μL of DNase I (ThermoFisher Scientific) using its buffer (10mM $MgCl_2$, 5mM $CaCl_2$
683 and 1μL of ribolock). Lysates were cleared by centrifugation at 16000 g, 10 min at 4°C.
684 Supernatants were precleared 1h at room temperature with magnetic beads blocked with BSA
685 (ThermoFisher Scientific) to avoid aspecific binding. Lysates were incubated overnight on
686 wheel at 4°C with immunoprecipitation buffer containing magnetic Protein A DynaBeads
687 (Invitrogen, ThermoFisher Scientific) conjugated with human PKR antibody (Abcam) or
688 negative control rabbit IgG (Cell signaling, Ozyme). Beads were washed 3 times with
689 immunoprecipitation buffer, 3 times with wash buffer (50mM tris-HCl [pH 7.5], 200mM NaCl,
690 5mM EDTA, 0.05% SDS, 1% triton, supplemented with Complete-EDTA-free Protease
691 Inhibitor Cocktail (complete Mini; Sigma Aldrich)) and twice with cold PBS 1X (Gibco®, Life
692 Technologies). Beads were eluted with 2x western blot loading buffer and incubated for 10 min
693 at 95°C under agitation. Proteins were analyzed by western blotting.
694
695 **RNase treatment followed by co-IP**
696 *On tagged proteins*: Cells were harvested, washed twice with ice-cold 1× PBS (Gibco®, Life
697 Technologies), and resuspended in 550 µL of lysis buffer (50 mM Tris-HCl pH 7.5, 140 mM
698 NaCl, 1.5 mM $MgCl_2$, 0.1% NP-40), supplemented with Complete-EDTA-free Protease
699 Inhibitor Cocktail (complete Mini; Sigma Aldrich). Cells were lysed by 30 min incubation on
700 ice and debris were removed by 15 min centrifugation at 2000 g and 4°C. Lysate was treated
701 or not with RNase A/T1 mix (ThermoFisher Scientific) and place at 37°C 30min. An aliquot of
702 the cleared lysates (25 µL) was kept aside as protein Input and another aliquot (25 µL) was kept
703 to assess RNase treatment efficiency. Co-IP was led as previously described.
704 Total RNA was extracted using Tri-Reagent Solution (Fisher Scientific; MRC, Inc) according
705 to the manufacturer's instructions. RNA integrity upon treatment was verified on an 1% agarose
706 gel containing ethidium bromide 10 mg/mL (Invitrogen, ThermoFisher Scientific) and revealed
707 under UV on Gel Doc™ EZ system (Bio-Rad).

708 **siRNA transfection**

709 20nM of human AGO2 or non-targeting control siRNA (Horizon discovery) were transfected
710 in 130 000 NoDice FHA:ctrl #2, NoDice FHA:DICER WT#4, N1 #6 or N3 #2.13 cells using
711 Lipofectamine 2000 transfection reagent (Invitrogen, ThermoFisher Scientific) according to the
712 manufacturer's instructions. After 24 hours, the cells were again transfected with 20nM of the
713 same siRNA and incubated overnight. Cells were infected or not with SINV-GFP at an MOI of
714 0.02 for 24h. Proteins and supernatants were collected and analyzed by western blotting and
715 plaque assay, respectively.

716

717 **BiFC assay**

718 Experiments were carried out in two different ways. For non-fixed cells, NoDiceΔPKR or
719 HEK293T cells were seeded at the density of 1.2 x 10^5 cells per well in a 24-well plate. After
720 16 hours, cells were transfected with equimolar quantities of each plasmid forming BiFC
721 couples. After 24 hours, cells were infected with SINV at an MOI of 2 and pictures were taken
722 6 hours post-infection using ZOE fluorescent cell imager (Bio-Rad). Proteins were collected
723 with lysis buffer (50 mM Tris-HCl pH 7.5, SDS 0.05%, Triton 1%, 5 mM EDTA, 150 mM
724 NaCl) supplemented with Complete-EDTA-free Protease Inhibitor Cocktail (complete Mini;
725 Sigma Aldrich), and subjected to western blot analysis. For fixed cells, NoDice/ΔPKR cells
726 were seeded at the density of 8.10^4 cells per well in 8-well Millicell® EZ Slides (Merck
727 Millipore), transfected and infected as described previously. At 6 hours post-infection, cells
728 were fixed with 4% formaldehyde and 0.2% glutaraldehyde for 10 min. Cells were then washed
729 with 1× PBS (Gibco®, Life Technologies) and stained with 10 μg/μL DAPI (Invitrogen,
730 ThermoFisher Scientific) in 1× PBS solution (Invitrogen, ThermoFisher Scientific) for 5 min.
731 Fixed cells were mounted on a glass slide with Fluoromount-G mounting media (Southern
732 Biotech). Images were acquired using confocal LSM780 (Zeiss) inverted microscope with an
733 argon laser (514x nm) and with ×40 immersion oil objective. All pictures obtained from BiFC
734 experiments were treated using FigureJ software (NIH).

735

736 **Mass spectrometry analysis**

737 Protein extracts were prepared for mass spectrometry as described in a previous study [87].
738 Each sample was precipitated with 0.1 M ammonium acetate in 100% methanol, and proteins
739 were resuspended in 50 mM ammonium bicarbonate. After a reduction-alkylation step
740 (dithiothreitol 5 mM – iodoacetamide 10 mM), proteins were digested overnight with

741 sequencing-grade porcine trypsin (1:25, w/w, Promega, Fitchburg, MA, USA). The resulting
742 vacuum-dried peptides were resuspended in water containing 0.1% (v/v) formic acid (solvent
743 A). One sixth of the peptide mixtures were analyzed by nanoLC-MS/MS an Easy-nanoLC-1000
744 system coupled to a Q-Exactive Plus mass spectrometer (Thermo-Fisher Scientific, USA)
745 operating in positive mode. Five microliters of each sample were loaded on a C-18 precolumn
746 (75 µm ID × 20 mm nanoViper, 3 μm Acclaim PepMap; Thermo) coupled with the analytical
747 C18 analytical column (75 µm ID × 25 cm nanoViper, 3 μm Acclaim PepMap; Thermo).
748 Peptides were eluted with a 160 min gradient of 0.1% formic acid in acetonitrile at 300 nL/min.
749 The Q-Exactive Plus was operated in data-dependent acquisition mode (DDA) with Xcalibur
750 software (Thermo-Fisher Scientific). Survey MS scans were acquired at a resolution of 70K at
751 200 m/z (mass range 350-1250), with a maximum injection time of 20 ms and an automatic
752 gain control (AGC) set to 3e6. Up to 10 of the most intense multiply charged ions (≥2) were
753 selected for fragmentation with a maximum injection time of 100 ms, an AGC set at 1e5 and a
754 resolution of 17.5K. A dynamic exclusion time of 20 s was applied during the peak selection
755 process.
756
757 **Database search and mass-spectrometry data post-processing**
758 Data were searched against a database containing Human and Viruses UniProtKB sequences
759 with a decoy strategy (GFP, Human and Sindbis Virus SwissProt sequences as well as Semliki
760 Forest Virus SwissProt and TrEMBL sequences (releases from January 2017, 40439
761 sequences)). Peptides were identified with Mascot algorithm (version 2.3, Matrix Science,
762 London, UK) with the following search parameters: carbamidomethylation of cysteine was set
763 as fixed modification; N-terminal protein acetylation, phosphorylation of serine / threonine /
764 tyrosine and oxidation of methionine were set as variable modifications; tryptic specificity with
765 up to three missed cleavages was used. The mass tolerances in MS and MS/MS were set to 10
766 ppm and 0.02 Da respectively, and the instrument configuration was specified as "ESI-Trap".
767 The resulting .dat Mascot files were then imported into Proline v1.4 package
768 (http://proline.profiproteomics.fr) for post-processing. Proteins were validated with Mascot
769 pretty rank equal to 1, 1% FDR on both peptide spectrum matches (PSM) and protein sets
770 (based on score). The total number of MS/MS fragmentation spectra (Spectral count or SpC)
771 was used for subsequent protein quantification in the different samples.
772
773 **Exploratory and differential expression analysis of LC-MS/MS data**

774 Mass spectrometry data obtained for each sample were stored in a local MongoDB database
775 and subsequently analyzed through a Shiny Application built upon the R/Bioconductor
776 packages msmsEDA (Gregori J, Sanchez A, Villanueva J (2014). msmsEDA: Exploratory Data
777 Analysis of LC-MS/MS data by spectral counts. R/Bioconductor package version 1.22.0) and
778 msmsTests (Gregori J, Sanchez A, Villanueva J (2013). msmsTests: LC-MS/MS Differential
779 Expression Tests. R/Bioconductor package version 1.22.0). Exploratory data analyses of LC-
780 MS/MS data were thus conducted, and differential expression tests were performed using a
781 negative binomial regression model. The p-values were adjusted with FDR control by the
782 Benjamini-Hochberg method and the following criteria were used to define differentially
783 expressed proteins: an adjusted p-value < 0.05, a minimum of 5 SpC in the most abundant
784 condition, and a minimum fold change of 2 (abs(LogFC) > 1). GO term analysis was performed
785 using the EnrichR web-based tool (http://amp.pharm.mssm.edu/Enrichr). The direct interaction
786 network for proteins enriched in SINV-infected cells was generated using the STRING database
787 (https://string-db.org).
788
789 **Data availability**
790 The mass spectrometry proteomics data have been deposited to the ProteomeXchange
791 Consortium via the PRIDE [88] partner repository with the dataset identifier PXD019093 and
792 10.6019/PXD019093.
793

794 ## Acknowledgments

795 The authors would like to thank members of the Pfeffer laboratory for discussion, Pr. Bryan
796 Cullen for the kind gift of the HEK293T NoDice and NoDice/ΔPKR cell lines and Dr. Oliver
797 Vugrek for the BiFC plasmids.
798 This work was funded by the European Research Council (ERC-CoG-647455 RegulRNA) and
799 was performed under the framework of the LABEX: ANR-10-LABX-0036_NETRNA and
800 ANR-17-EURE-0023, which benefits from a funding from the state managed by the French
801 National Research Agency as part of the Investments for the future program. This work has
802 also received funding from the People Programme (Marie Curie Actions) of the European
803 Union's Seventh Framework Program (FP7/2007-2013) under REA grant agreement n°
804 PCOFUND-GA-2013-609102, through the PRESTIGE program coordinated by Campus
805 France (to EG), and from the French Minister for Higher Education, Research and Innovation

(PhD contract to MB). The mass spectrometry instrumentation was funded by the University of Strasbourg, IdEx “Equipement mi-lourd” 2015.

Author contributions

SP and ML conceived the project. TCM, ML, EG and SP designed the work. TCM, MB, ML, EG and MM performed the experiments and analyzed the results. PH and JC performed the mass spectrometry analysis. BCWM designed software and analyzed the mass spectrometry results. SP coordinated the work and assured funding. TCM, MB and SP wrote the manuscript with input from the other authors. All authors reviewed and approved the final manuscript.

References

1. Ivashkiv LB, Donlin LT. Regulation of type I interferon responses. Nat Rev Immunol. 2014;14: 36–49. doi:10.1038/nri3581
2. Borden EC, Sen GC, Uze G, Silverman RH, Ransohoff RM, Foster GR, et al. Interferons at age 50: past, current and future impact on biomedicine. Nat Rev Drug Discov. 2007;6: 975–990. doi:10.1038/nrd2422
3. Williams BR. PKR; a sentinel kinase for cellular stress. Oncogene. 1999;18: 6112–6120. doi:10.1038/sj.onc.1203127
4. Lemaire PA, Anderson E, Lary J, Cole JL. Mechanism of PKR Activation by dsRNA. J Mol Biol. 2008;381: 351–360. doi:10.1016/j.jmb.2008.05.056
5. Pfaller CK, Li Z, George CX, Samuel CE. Protein kinase PKR and RNA adenosine deaminase ADAR1: new roles for old players as modulators of the interferon response. Curr Opin Immunol. 2011;23: 573–582. doi:10.1016/j.coi.2011.08.009
6. Fros JJ, Pijlman GP. Alphavirus Infection: Host Cell Shut-Off and Inhibition of Antiviral Responses. Viruses. 2016;8: 166. doi:10.3390/v8060166
7. Ryman KD, White LJ, Johnston RE, Klimstra WB. Effects of PKR/RNase L-Dependent and Alternative Antiviral Pathways on Alphavirus Replication and Pathogenesis. Viral Immunol. 2002;15: 53–76. doi:10.1089/088282402317340233
8. Kim Y, Lee JH, Park J-E, Cho J, Yi H, Kim VN. PKR is activated by cellular dsRNAs during mitosis and acts as a mitotic regulator. Genes Dev. 2014;28: 1310–1322. doi:10.1101/gad.242644.114
9. Meister G, Tuschl T. Mechanisms of gene silencing by double-stranded RNA. Nature. 2004;431: 343–9. doi:10.1038/nature02873
10. Hutvágner G, McLachlan J, Pasquinelli AE, Balint E, Tuschl T, Zamore PD. A cellular function for the RNA-interference enzyme Dicer in the maturation of the let-7 small temporal RNA. Science. 2001;293: 834–8. doi:10.1126/science.1062961
11. Wienholds E, Koudijs MJ, Van Eeden FJ, Cuppen E, Plasterk RH. The microRNA-producing enzyme Dicer1 is essential for zebrafish development. Nat Genet. 2003; 217–218. doi:10.1038/ng1251
12. Bartel DP. Metazoan MicroRNAs. Cell. 2018;173: 20–51. doi:10.1016/j.cell.2018.03.006
13. Chendrimada TP, Gregory RI, Kumaraswamy E, Norman J, Cooch N, Nishikura K, et al. TRBP recruits the Dicer complex to Ago2 for microRNA processing and gene silencing. Nature. 2005;436: 740–4. doi:10.1038/nature03868
14. Daniels SM, Melendez-Peña CE, Scarborough RJ, Daher A, Christensen HS, El Far M, et al. Characterization of the TRBP domain required for dicer interaction and function in RNA interference. BMC Mol Biol. 2009;10: 38. doi:10.1186/1471-2199-10-38
15. Heyam A, Lagos D, Plevin M. Dissecting the roles of TRBP and PACT in double-stranded RNA recognition and processing of noncoding RNAs. WIREs RNA. 2015;6: 271–289. doi:10.1002/wrna.1272
16. Kok KH, Ng MH, Ching YP, Jin DY. Human TRBP and PACT Directly Interact with Each Other and Associate with Dicer to Facilitate the Production of Small Interfering RNA. J Biol Chem. 2007;282: 17649–57. doi:10.1074/jbc.M611768200
17. Lee Y, Hur I, Park SY, Kim YK, Suh MR, Kim VN. The role of PACT in the RNA silencing pathway. Embo J. 2006;25: 522–32. doi:10.1038/sj.emboj.7600942
18. Guo Z, Li Y, Ding S-W. Small RNA-based antimicrobial immunity. Nat Rev Immunol. 2019;19: 31–44. doi:10.1038/s41577-018-0071-x
19. tenOever BR. The Evolution of Antiviral Defense Systems. Cell Host Microbe. 2016;19: 142–149. doi:10.1016/j.chom.2016.01.006
20. Cullen BR. Is RNA interference involved in intrinsic antiviral immunity in mammals? Nat

865 Immunol. 2006;7: 563–7. doi:10.1038/ni1352
866 21. Maillard PV, van der Veen AG, Poirier EZ, Reis e Sousa C. Slicing and dicing viruses:
867 antiviral RNA interference in mammals. EMBO J. 2019;38.
868 doi:10.15252/embj.2018100941
869 22. Maillard PV, Ciaudo C, Marchais A, Li Y, Jay F, Ding SW, et al. Antiviral RNA
870 interference in mammalian cells. Science. 2013;342: 235–238.
871 doi:10.1126/science.1241930
872 23. Maillard PV, Veen AGV der, Deddouche-Grass S, Rogers NC, Merits A, Sousa CR e.
873 Inactivation of the type I interferon pathway reveals long double-stranded RNA-mediated
874 RNA interference in mammalian cells. EMBO J. 2016;35: 2505–2518.
875 doi:10.15252/embj.201695086
876 24. Takahashi T, Nakano Y, Onomoto K, Murakami F, Komori C, Suzuki Y, et al. LGP2 virus
877 sensor regulates gene expression network mediated by TRBP-bound microRNAs. Nucleic
878 Acids Res. 2018;46: 9134–9147. doi:10.1093/nar/gky575
879 25. Takahashi T, Nakano Y, Onomoto K, Yoneyama M, Ui-Tei K. Virus Sensor RIG-I
880 Represses RNA Interference by Interacting with TRBP through LGP2 in Mammalian
881 Cells. Genes. 2018;9: 511. doi:10.3390/genes9100511
882 26. van der Veen AG, Maillard PV, Schmidt JM, Lee SA, Deddouche-Grass S, Borg A, et al.
883 The RIG-I-like receptor LGP2 inhibits Dicer-dependent processing of long double-
884 stranded RNA and blocks RNA interference in mammalian cells. EMBO J. 2018;37:
885 e97479. doi:10.15252/embj.201797479
886 27. Adiliaghdam F, Basavappa M, Saunders TL, Harjanto D, Prior JT, Cronkite DA, et al. A
887 Requirement for Argonaute 4 in Mammalian Antiviral Defense. Cell Rep. 2020;30: 1690-
888 1701.e4. doi:10.1016/j.celrep.2020.01.021
889 28. Qiu Y, Xu Y, Zhang Y, Zhou H, Deng Y-Q, Li X-F, et al. Human Virus-Derived Small
890 RNAs Can Confer Antiviral Immunity in Mammals. Immunity. 2017;46: 992-1004.e5.
891 doi:10.1016/j.immuni.2017.05.006
892 29. Qiu Y, Xu Y-P, Wang M, Miao M, Zhou H, Xu J, et al. Flavivirus induces and antagonizes
893 antiviral RNA interference in both mammals and mosquitoes. Sci Adv. 2020;6: eaax7989.
894 doi:10.1126/sciadv.aax7989
895 30. Girardi E, Chane-Woon-Ming B, Messmer M, Kaukinen P, Pfeffer S. Identification of
896 RNase L-dependent, 3'-end-modified, viral small RNAs in Sindbis virus-infected
897 mammalian cells. mBio. 2013;4: e00698-00613. doi:10.1128/mBio.00698-13
898 31. Parameswaran P, Sklan E, Wilkins C, Burgon T, Samuel MA, Lu R, et al. Six RNA viruses
899 and forty-one hosts: viral small RNAs and modulation of small RNA repertoires in
900 vertebrate and invertebrate systems. PLoS Pathog. 2010;6: e1000764.
901 doi:10.1371/journal.ppat.1000764
902 32. Schuster S, Overheul GJ, Bauer L, van Kuppeveld FJM, van Rij RP. No evidence for viral
903 small RNA production and antiviral function of Argonaute 2 in human cells. Sci Rep.
904 2019;9: 1–11. doi:10.1038/s41598-019-50287-w
905 33. Kennedy EM, Whisnant AW, Kornepati AVR, Marshall JB, Bogerd HP, Cullen BR.
906 Production of functional small interfering RNAs by an amino-terminal deletion mutant of
907 human Dicer. Proc Natl Acad Sci. 2015;112: E6945–E6954.
908 doi:10.1073/pnas.1513421112
909 34. Tsai K, Courtney DG, Kennedy EM, Cullen BR. Influenza A virus-derived siRNAs
910 increase in the absence of NS1 yet fail to inhibit virus replication. RNA N Y N. 2018.
911 doi:10.1261/rna.066332.118
912 35. Griffin D. Alphaviruses, p 1023–1067. Fields Virol 5th Ed Lippincott Williams Wilkins
913 Phila PA. 2007.
914 36. Girardi E, Lefèvre M, Chane-Woon-Ming B, Paro S, Claydon B, Imler J-L, et al. Cross-

species comparative analysis of Dicer proteins during Sindbis virus infection. Sci Rep. 2015;5: 10693. doi:10.1038/srep10693

37. Bogerd HP, Skalsky RL, Kennedy EM, Furuse Y, Whisnant AW, Flores O, et al. Replication of many human viruses is refractory to inhibition by endogenous cellular microRNAs. J Virol. 2014;88: 8065–8076. doi:10.1128/JVI.00985-14
38. López P, Girardi E, Mounce BC, Weiss A, Chane-Woon-Ming B, Messmer M, et al. High-Throughput Fluorescence-Based Screen Identifies the Neuronal MicroRNA miR-124 as a Positive Regulator of Alphavirus Infection. J Virol. 2020;94. doi:10.1128/JVI.02145-19
39. Bogerd HP, Whisnant AW, Kennedy EM, Flores O, Cullen BR. Derivation and characterization of Dicer- and microRNA-deficient human cells. RNA. 2014;20: 923–937. doi:10.1261/rna.044545.114
40. Aktaş T, Avşar Ilık İ, Maticzka D, Bhardwaj V, Pessoa Rodrigues C, Mittler G, et al. DHX9 suppresses RNA processing defects originating from the Alu invasion of the human genome. Nature. 2017;544: 115–119. doi:10.1038/nature21715
41. Robb GB, Rana TM. RNA helicase A interacts with RISC in human cells and functions in RISC loading. Mol Cell. 2007;26: 523–537. doi:10.1016/j.molcel.2007.04.016
42. Sorrentino S, Naddeo M, Russo A, D'Alessio G. Degradation of double-stranded RNA by human pancreatic ribonuclease: crucial role of noncatalytic basic amino acid residues. Biochemistry. 2003;42: 10182–10190. doi:10.1021/bi030040q
43. Edy VG, Szekely M, Loviny T, Dreyer C. Action of nucleases on double-stranded RNA. Eur J Biochem. 1976;61: 563–572. doi:10.1111/j.1432-1033.1976.tb10051.x
44. García MA, Meurs EF, Esteban M. The dsRNA protein kinase PKR: Virus and cell control. Biochimie. 2007;89: 799–811. doi:10.1016/j.biochi.2007.03.001
45. Haase AD, Jaskiewicz L, Zhang H, Laine S, Sack R, Gatignol A, et al. TRBP, a regulator of cellular PKR and HIV-1 virus expression, interacts with Dicer and functions in RNA silencing. EMBO Rep. 2005;6: 961–7. doi:10.1038/sj.embor.7400509
46. Patel CV, Handy I, Goldsmith T, Patel RC. PACT, a Stress-modulated Cellular Activator of Interferon-induced Double-stranded RNA-activated Protein Kinase, PKR. J Biol Chem. 2000;275: 37993–37998. doi:10.1074/jbc.M004762200
47. Lepur A, Kovačević L, Belužić R, Vugrek O. Combining unique multiplex gateway cloning and bimolecular fluorescence complementation (BiFC) for high-throughput screening of protein–protein interactions. J Biomol Screen. 2016;21: 1100–1111. doi:10.1177/1087057116659438
48. Bernstein E, Caudy AA, Hammond SM, Hannon GJ. Role for a bidentate ribonuclease in the initiation step of RNA interference. Nature. 2001;409: 363–6. doi:10.1038/35053110
49. Doyle M, Badertscher L, Jaskiewicz L, Güttinger S, Jurado S, Hugenschmidt T, et al. The double-stranded RNA binding domain of human Dicer functions as a nuclear localization signal. RNA N Y N. 2013;19: 1238–1252. doi:10.1261/rna.039255.113
50. Lambert M, Pépin G, Peralta-Zaragoza O, Matusiak R, Ly S, Landry P, et al. TWEAK Negatively Regulates Human Dicer. Non-Coding RNA. 2016;2. doi:10.3390/ncrna2040012
51. Meister G, Landthaler M, Patkaniowska A, Dorsett Y, Teng G, Tuschl T. Human Argonaute2 mediates RNA cleavage targeted by miRNAs and siRNAs. Mol Cell. 2004;15: 185–197. doi:10.1016/j.molcel.2004.07.007
52. Li Y, Basavappa M, Lu J, Dong S, Cronkite DA, Prior JT, et al. Induction and suppression of antiviral RNA interference by influenza A virus in mammalian cells. Nat Microbiol. 2016;2: 16250. doi:10.1038/nmicrobiol.2016.250
53. Cullen BR, Cherry S, tenOever BR. Is RNA Interference a Physiologically Relevant Innate Antiviral Immune Response in Mammals? Cell Host Microbe. 2013;14: 374–378. doi:10.1016/j.chom.2013.09.011

965 54. Cullen BR. RNA Interference in Mammals: The Virus Strikes Back. Immunity. 2017;46:
966 970–972. doi:10.1016/j.immuni.2017.05.004
967 55. Donaszi-Ivanov A, Mohorianu I, Dalmay T, Powell PP. Small RNA Analysis in Sindbis
968 Virus Infected Human HEK293 Cells. Adelman ZN, editor. PLoS ONE. 2013;8: e84070.
969 doi:10.1371/journal.pone.0084070
970 56. Backes S, Langlois RA, Schmid S, Varble A, Shim JV, Sachs D, et al. The Mammalian
971 Response to Virus Infection Is Independent of Small RNA Silencing. Cell Rep. 2014;8:
972 114–125. doi:10.1016/j.celrep.2014.05.038
973 57. Li Y, Lu J, Han Y, Fan X, Ding S-W. RNA interference functions as an antiviral immunity
974 mechanism in mammals. Science. 2013;342: 231–234. doi:10.1126/science.1241911
975 58. Berkhout B. RNAi-mediated antiviral immunity in mammals. Curr Opin Virol. 2018;32:
976 9–14. doi:10.1016/j.coviro.2018.07.008
977 59. Takahashi T, Ui-Tei K. Mutual Regulation of RNA Silencing and the IFN Response as an
978 Antiviral Defense System in Mammalian Cells. Int J Mol Sci. 2020;21: 1348.
979 doi:10.3390/ijms21041348
980 60. Lui P-Y, Wong L-YR, Ho T-H, Au SWN, Chan C-P, Kok K-H, et al. PACT Facilitates
981 RNA-Induced Activation of MDA5 by Promoting MDA5 Oligomerization. J Immunol.
982 2017;199: 1846–1855. doi:10.4049/jimmunol.1601493
983 61. Kok K-H, Lui P-Y, Ng M-HJ, Siu K-L, Au SWN, Jin D-Y. The Double-Stranded RNA-
984 Binding Protein PACT Functions as a Cellular Activator of RIG-I to Facilitate Innate
985 Antiviral Response. Cell Host Microbe. 2011;9: 299–309.
986 doi:10.1016/j.chom.2011.03.007
987 62. Clemens MJ. PKR-a protein kinase regulated by double-stranded RNA. Int J Biochem Cell
988 Biol. 1997;29: 945–9. doi:10.1016/s1357-2725(96)00169-0
989 63. Gal-Ben-Ari S, Barrera I, Ehrlich M, Rosenblum K. PKR: A Kinase to Remember. Front
990 Mol Neurosci. 2018;11: 480. doi:10.3389/fnmol.2018.00480
991 64. Fairman-Williams ME, Guenther U-P, Jankowsky E. SF1 and SF2 helicases: family
992 matters. Curr Opin Struct Biol. 2010;20: 313–324. doi:10.1016/j.sbi.2010.03.011
993 65. Ahmad S, Hur S. Helicases in Antiviral Immunity: Dual Properties as Sensors and
994 Effectors. Trends Biochem Sci. 2015;40: 576–585. doi:10.1016/j.tibs.2015.08.001
995 66. Mittelstadt M, Frump A, Khuu T, Fowlkes V, Handy I, Patel CV, et al. Interaction of
996 human tRNA-dihydrouridine synthase-2 with interferon-induced protein kinase PKR.
997 Nucleic Acids Res. 2008;36: 998–1008. doi:10.1093/nar/gkm1129
998 67. Park H, Davies MV, Langland JO, Chang HW, Nam YS, Tartaglia J, et al. TAR RNA-
999 binding protein is an inhibitor of the interferon-induced protein kinase PKR. Proc Natl
1000 Acad Sci U S A. 1994;91: 4713–4717. doi:10.1073/pnas.91.11.4713
1001 68. Nakamura T, Kunz RC, Zhang C, Kimura T, Yuan CL, Baccaro B, et al. A Critical Role
1002 for PKR Complexes with TRBP in Immunometabolic Regulation and eIF2α
1003 Phosphorylation in Obesity. Cell Rep. 2015;11: 295–307.
1004 doi:10.1016/j.celrep.2015.03.021
1005 69. Daher A, Laraki G, Singh M, Melendez-Peña CE, Bannwarth S, Peters AHFM, et al. TRBP
1006 control of PACT-induced phosphorylation of protein kinase R is reversed by stress. Mol
1007 Cell Biol. 2009;29: 254–265. doi:10.1128/MCB.01030-08
1008 70. Singh M, Castillo D, Patel CV, Patel RC. Stress-induced phosphorylation of PACT reduces
1009 its interaction with TRBP and leads to PKR activation. Biochemistry. 2011;50: 4550–4560.
1010 doi:10.1021/bi200104h
1011 71. Clerzius G, Shaw E, Daher A, Burugu S, Gélinas J-F, Ear T, et al. The PKR activator,
1012 PACT, becomes a PKR inhibitor during HIV-1 replication. Retrovirology. 2013;10: 96.
1013 doi:10.1186/1742-4690-10-96
1014 72. Li J, Tang H, Mullen TM, Westberg C, Reddy TR, Rose DW, et al. A role for RNA helicase

A in post-transcriptional regulation of HIV type 1. Proc Natl Acad Sci U S A. 1999;96: 709–714. doi:10.1073/pnas.96.2.709

73. Fujii R, Okamoto M, Aratani S, Oishi T, Ohshima T, Taira K, et al. A Role of RNA Helicase A in cis-Acting Transactivation Response Element-mediated Transcriptional Regulation of Human Immunodeficiency Virus Type 1. J Biol Chem. 2001;276: 5445–5451. doi:10.1074/jbc.M006892200
74. Roy BB, Hu J, Guo X, Russell RS, Guo F, Kleiman L, et al. Association of RNA helicase a with human immunodeficiency virus type 1 particles. J Biol Chem. 2006;281: 12625–12635. doi:10.1074/jbc.M510596200
75. Sadler AJ, Latchoumanin O, Hawkes D, Mak J, Williams BRG. An Antiviral Response Directed by PKR Phosphorylation of the RNA Helicase A. Gale M, editor. PLoS Pathog. 2009;5: e1000311. doi:10.1371/journal.ppat.1000311
76. Herbert A, Alfken J, Kim YG, Mian IS, Nishikura K, Rich A. A Z-DNA binding domain present in the human editing enzyme, double-stranded RNA adenosine deaminase. Proc Natl Acad Sci U S A. 1997;94: 8421–8426. doi:10.1073/pnas.94.16.8421
77. Yang W, Chendrimada TP, Wang Q, Higuchi M, Seeburg PH, Shiekhattar R, et al. Modulation of microRNA processing and expression through RNA editing by ADAR deaminases. Nat Struct Mol Biol. 2006;13: 13–21. doi:10.1038/nsmb1041
78. Iizasa H, Wulff B-E, Alla NR, Maragkakis M, Megraw M, Hatzigeorgiou A, et al. Editing of Epstein-Barr virus-encoded BART6 microRNAs controls their dicer targeting and consequently affects viral latency. J Biol Chem. 2010;285: 33358–33370. doi:10.1074/jbc.M110.138362
79. Ota H, Sakurai M, Gupta R, Valente L, Wulff B-E, Ariyoshi K, et al. ADAR1 forms a complex with Dicer to promote microRNA processing and RNA-induced gene silencing. Cell. 2013;153: 575–589. doi:10.1016/j.cell.2013.03.024
80. Samuel CE. Adenosine deaminases acting on RNA (ADARs) are both antiviral and proviral. Virology. 2011;411: 180–193. doi:10.1016/j.virol.2010.12.004
81. Li Z, Wolff KC, Samuel CE. RNA adenosine deaminase ADAR1 deficiency leads to increased activation of protein kinase PKR and reduced vesicular stomatitis virus growth following interferon treatment. Virology. 2010;396: 316–322. doi:10.1016/j.virol.2009.10.026
82. Clerzius G, Gélinas J-F, Daher A, Bonnet M, Meurs EF, Gatignol A. ADAR1 interacts with PKR during human immunodeficiency virus infection of lymphocytes and contributes to viral replication. J Virol. 2009;83: 10119–10128. doi:10.1128/JVI.02457-08
83. Schoggins JW, Wilson SJ, Panis M, Murphy MY, Jones CT, Bieniasz P, et al. A diverse range of gene products are effectors of the type I interferon antiviral response. Nature. 2011;472: 481–485. doi:10.1038/nature09907
84. Elde NC, Child SJ, Geballe AP, Malik HS. Protein kinase R reveals an evolutionary model for defeating viral mimicry. Nature. 2009;457: 485–489. doi:10.1038/nature07529
85. Meister G, Landthaler M, Peters L, Chen PY, Urlaub H, Lührmann R, et al. Identification of novel argonaute-associated proteins. Curr Biol CB. 2005;15: 2149–2155. doi:10.1016/j.cub.2005.10.048
86. Concordet J-P, Haeussler M. CRISPOR: intuitive guide selection for CRISPR/Cas9 genome editing experiments and screens. Nucleic Acids Res. 2018;46: W242–W245. doi:10.1093/nar/gky354
87. Chicois C, Scheer H, Garcia S, Zuber H, Mutterer J, Chicher J, et al. The UPF1 interactome reveals interaction networks between RNA degradation and translation repression factors in Arabidopsis. Plant J. 2018;96: 119–132. doi:10.1111/tpj.14022
88. Perez-Riverol Y, Csordas A, Bai J, Bernal-Llinares M, Hewapathirana S, Kundu DJ, et al. The PRIDE database and related tools and resources in 2019: improving support for

1065 quantification data. Nucleic Acids Res. 2019;47: D442–D450. doi:10.1093/nar/gky1106
1066 89. Chen EY, Tan CM, Kou Y, Duan Q, Wang Z, Meirelles GV, et al. Enrichr: interactive and
1067 collaborative HTML5 gene list enrichment analysis tool. BMC Bioinformatics. 2013;14:
1068 128. doi:10.1186/1471-2105-14-128
1069 90. Kuleshov MV, Jones MR, Rouillard AD, Fernandez NF, Duan Q, Wang Z, et al. Enrichr:
1070 a comprehensive gene set enrichment analysis web server 2016 update. Nucleic Acids Res.
1071 2016;44: W90-97. doi:10.1093/nar/gkw377
1072

1073 ## Figure legends

1074 **Figure 1. Analysis of SINV infection in HEK293T cells and characterization of**
1075 **FHA:DICER WT cell lines**

1076 **A.** GFP fluorescent microscopy pictures of HEK293T, NoDice FHA:ctrl #1 and FHA:DICER
1077 cell lines infected (polyclonal and two clones, #4 and #17) with SINV-GFP at an MOI of 0.02
1078 for 24 h. The left panel corresponds to GFP signal from infected cells and the right panel to a
1079 merge picture of GFP signal and brightfield. Pictures were taken with a 5x magnification. hpi:
1080 hours post-infection. **B.** Western blot analysis of DICER (DICER and HA) and GFP expression
1081 in SINV-GFP-infected HEK293T, NoDice FHA:ctrl #1 and FHA:DICER cell lines shown in
1082 **A**. Gamma-Tubulin was used as loading control. **C.** Mean (+/- SEM) of SINV-GFP viral titers
1083 in the same cell lines as in **A** infected at an MOI of 0.02 for 24 h (n = 3) from plaque assay
1084 quantification. ns: non-significant, ordinary one-way ANOVA test with Bonferroni correction.
1085 **D.** Western blot analysis of DICER (DICER and HA) and AGO2 expression in HEK293T,
1086 NoDice FHA:ctrl #1 and FHA:DICER cell lines. Gamma-Tubulin was used as loading control.
1087

1088 **Figure 2. LC-MS/MS analysis of DICER interactome during SINV infection**

1089 **A.** Volcano plot for differentially expressed proteins (DEPs) between HA IP and CTL IP in
1090 FHA:DICER mock-infected cells. Each protein is marked as a dot; proteins that are
1091 significantly up-regulated in HA IP are shown in red, up-regulated proteins in CTL IP are
1092 shown in blue, and non-significant proteins are in black. The horizontal line denotes a p-value
1093 of 0.05 and the vertical lines the Log2 fold change cutoff (-1 and 1). DICER and its cofactors
1094 (TRBP, PACT, AGO2) are highlighted in yellow. **B.** Volcano plot for DEPs between SINV-
1095 GFP (MOI of 2, 6 hpi) and mock fractions of HA IP in FHA:DICER cells. Same colour code
1096 and thresholds as in A have been applied. Proteins that are discussed in the text are highlighted
1097 in yellow and SINV proteins in purple. **C.** Gene Ontology (GO) term enrichment of proteins
1098 up-regulated in SINV-GFP fraction of HA IP using Enrichr software [89,90]. The graph
1099 displays the GO term hierarchy within the "biological process" branch sorted by p-value
1100 ranking computed from the Fisher exact test. The length of each bar represents the significance
1101 of that specific term. In addition, the brighter the colour is, the more significant that term is.
1102 Viral proteins have been excluded for this analysis. **D.** STRING interaction network of the top
1103 100 proteins enriched in SINV-infected vs. mock-infected cells. Proteins involved in RNA
1104 metabolic processes or the regulation thereof are indicated in red and blue respectively, proteins
1105 with a known dsRNA binding function are indicated in green. DICER is indicated by a red

1106 circle. **E.** Summary of the differential expression analysis of SINV-GFP vs mock fractions from
1107 HA IP in FHA:DICER cells. The analysis has been performed using a generalized linear model
1108 of a negative-binomial distribution and p-values were corrected for multiple testing using the
1109 Benjamini-Hochberg method.
1110
1111 **Figure 3. Confirmation of LC-MS/MS analysis by co-IP and BiFC**
1112 **A.** Western blot analysis of HA co-IP in mock or SINV-GFP-infected (MOI of 2, 6 hpi)
1113 FHA:DICER WT #4 cells. Proteins associated to FHA:DICER were revealed by using
1114 antibodies targeting endogenous ADAR-1, PKR, TRBP, DHX9 or PACT proteins. In parallel,
1115 an HA antibody was used to verify the IP efficiency and GFP antibody was used to verify the
1116 infection. Ponceau was used as loading control. **B.** Western blot analysis of HA co-IP in mock
1117 or SINV-GFP-infected (MOI of 2, 6 hpi) FHA:DICER WT #4 cells. The lysate was treated or
1118 not with RNase A/T1. Proteins associated to FHA:DICER were revealed by using antibodies
1119 targeting endogenous DHX9, p-PKR, PKR, TRBP, or PACT proteins. In parallel, an HA
1120 antibody was used to verify the IP efficiency and GFP antibody was used to verify the infection.
1121 Ponceau was used as loading control. The arrow points to the expected size of the FHA:DICER
1122 protein and the asterisks correspond to aspecific bands. **C.** Western blot analysis to validate the
1123 interaction of PKR with DICER (upper panel) and PACT (lower panel) in mock or SINV-GFP-
1124 infected HEK293T cells (MOI of 2, 6 hpi). Immunoprecipitated proteins obtained from PKR
1125 pulldowns were compared to rabbit IgG pulldowns to verify the specificity of the assay. **D.**
1126 Interactions between DICER and TRBP, PACT or PKR were visualized by BiFC. Plasmids
1127 expressing $^{N\text{-}ter}$Venus:DICER and TRBP:, PACT: or PKR:Venus$^{C\text{-}ter}$ were co-transfected in
1128 NoDice/ΔPKR cells for 24 h and cells were either infected with SINV at an MOI of 2 for 6 h
1129 or not. The different combinations are indicated on the left side. Reconstitution of Venus (BiFC)
1130 signal was observed under epifluorescence microscope. For each condition, the left panel
1131 corresponds to Venus signal and the right panel to the corresponding brightfield pictures. Scale
1132 bar: 100 µm. hpi: hours post-infection. **E.** BiFC experiment on fixed NoDice/ΔPKR cells
1133 treated as in D. After fixation, cells were stained with DAPI and observed under confocal
1134 microscope. Only a merge picture of BiFC and DAPI signals of SINV-infected cells is shown
1135 here. A higher magnification of picture showing cytoplasmic localization of the interaction
1136 represented by a red square is shown in the bottom left corner. Scale bar: 20 µm and 10 µm.
1137

1138 **Figure 4. Confirmation of DICER interactome upon SINV infection in HCT116 KI-**
1139 **DICER cells**
1140 **A.** Western blot analysis of DICER, AGO2, PKR and TRBP expression in HEK293T, HCT116
1141 and HCT116 KI-DICER cell lines. Gamma-Tubulin and ponceau were used as loading control.
1142 **B**. GFP fluorescent microscopy pictures of HEK293T, HCT116 and HCT116 KI-DICER cell
1143 lines infected with SINV-GFP at an MOI of 0.02, 0.1 and 1 for 24 h. The left panel corresponds
1144 to GFP signal from infected cells and the right panel to a merge picture of GFP signal and
1145 brightfield. Pictures were taken with a 5x magnification. **C**. miR-16 expression analyzed by
1146 northern blot in in the same cell lines as in B. Expression of snRNA U6 was used as loading
1147 control. **D.** Western blot analysis of HA co-IP in mock or SINV-GFP-infected (MOI of 0.1, 24
1148 hpi) HCT116 KI-DICER cells. Proteins associated to FHA-GFP:DICER were revealed by using
1149 antibodies targeting endogenous DHX9, p-PKR, PKR, PACT or TRBP proteins. The TRBP
1150 immunoblot was performed by loading the same samples on a separate membrane. In parallel,
1151 an HA antibody was used to verify the IP efficiency and GFP antibody was used to verify the
1152 infection. Ponceau was used as a loading control.
1153
1154 **Figure 5. Identification of DICER domains involved in DICER-PKR interaction**
1155 **A.** Schematic representation of Human DICER proteins used in this study. The different
1156 conserved domains are shown in colored boxes. DUF283: Domain of Unknown Function; PAZ:
1157 PIWI ARGONAUTE ZWILLE domain; dsRBD: dsRNA-binding domain. hDICER WT is the
1158 full-length protein. hDICER N1 is deleted of the first N-terminal 495 amino acids. hDICER N3
1159 is wholly deleted of the helicase domain. hDICER Hel. is the whole DICER's helicase domain.
1160 hDICER ΔdsRBD is deleted of the C-terminal dsRBD. **B.** Western blot analysis of HA co-IP
1161 in mock NoDice 2.20 cells transfected with different versions of FHA:DICER proteins.
1162 Efficiency of immunoprecipitation was assessed using anti-HA and anti-DICER antibodies and
1163 co-IPs of TRBP, PKR and PACT were examined using appropriate antibodies. Expression of
1164 GFP in INPUT fraction was visualized as control of SINV-GFP infection. Ponceau staining of
1165 membranes is used as loading control. **C.** Western blot analysis of HA co-IP in NoDice 2.20
1166 cells transfected with different versions of FHA:DICER proteins and infected with SINV-GFP
1167 (MOI of 2, 6 hpi). Efficiency of immunoprecipitation was assessed using an anti- Flag antibody
1168 and co-IPs of PKR, TRBP, p-PKR and PACT were examined using appropriate antibodies.
1169 Expression of GFP in INPUT fraction was visualized as control of SINV-GFP infection.
1170 Ponceau staining of membranes is used as loading control. The DICER Hel. band is indicated
1171 by a red asterisk. **D.** Plasmids expressing the different versions of DICER proteins fused to the

1172 N-terminal part of Venus and PKR:Venus$^{C\text{-}ter}$ plasmid were co-transfected in NoDice/ΔPKR
1173 cells. Cells were treated as in Fig. 3D. The different combinations are noted on the left side.
1174 The fluorescent signal was observed using an epifluorescence microscope. For each condition,
1175 the left panel corresponds to Venus signal and the right panel to the corresponding brightfield
1176 pictures. Scale bar: 100 μm. hpi: hours post-infection.
1177
1178 **Figure 6. Analysis of the importance of Dicer helicase domain on SINV-GFP infection in**
1179 **FHA:DICER mutant stable cell lines**
1180 **A.** Expression of DICER (DICER, HA), TRBP and AGO2 was analysed by western blot in
1181 HEK293T, NoDice FHA:ctrl #1, FHA:DICER WT #4 and FHA:DICER N1 #6 cell lines.
1182 Gamma-Tubulin was used as loading control. **B.** Northern blot analysis of miR-16 expression
1183 in the same samples as in A. Expression of snRNA U6 was used as loading control. **C.**
1184 Representative GFP fluorescent microscopy images of HEK293T, FHA:DICER WT #4 and
1185 FHA:DICER N1 #6 cell lines infected with SINV-GFP at an MOI of 0.02 for 24 h. The left
1186 panel corresponds to GFP signal and the right panel to a merge picture of GFP signal and
1187 brightfield. Pictures were taken with a 5x magnification. hpi: hours post-infection. **D.** Western
1188 blot analysis of DICER (DICER and HA), AGO2, PKR, and GFP expression in SINV-GFP-
1189 infected cells in the same condition as in C. Gamma-Tubulin was used as loading control. The
1190 asterisk correspond to aspecific bands **E.** Mean (+/- SEM) of SINV-GFP viral titers fold change
1191 over HEK293T cells in HEK293T, NoDice 2.20, FHA:DICER WT #4 and FHA:DICER
1192 mutants cell lines infected at an MOI of 0.02 for 24 h (n = 3) from plaque assay quantification.
1193 * $p < 0.05$, ns: non-significant, ordinary one-way ANOVA test with Bonferroni correction.
1194
1195 **Figure 7. The antiviral effect of helicase-deleted DICER mutants is independent from**
1196 **AGO2**
1197 **A.** GFP fluorescent microscopy pictures of NoDice FHA:ctrl #2, NoDice FHA:DICER WT #4
1198 and NoDice FHA:DICER mutant cell lines treated with two doses of siAGO2 at 20nM for 48
1199 hours before a 24-hour-SINV-GFP infection at an MOI of 0.02. The left panel corresponds to
1200 GFP signal from infected cells and the right panel to a merge picture of GFP signal and
1201 brightfield. Pictures were taken with 5x magnification. hpi: hours post-infection. **B.** Western
1202 blot analysis of DICER, AGO2 and GFP expression in SINV GFP-infected NoDice FHA:ctrl
1203 #2, NoDice FHA:DICER WT #4 and NoDice FHA:DICER mutant cell lines shown in **A**. Cells
1204 were treated with two doses of siAGO2 at 20nM for 48 hours before a 24-hour-SINV-GFP

1205 infection at an MOI of 0.02. Gamma-Tubulin was used as loading control. **C.** Mean (+/-SEM)
1206 of SINV-GFP viral titers in the same cell lines as in **A.** infected at an MOI of 0.02 for 24h (n =
1207 3) from plaque assay quantification. ns: non-significant, two-tailed unpaired parametric t-test.
1208
1209 **Figure 8. The antiviral effect of helicase-deleted DICER mutants requires PKR**
1210 **A.** GFP fluorescent microscopy pictures of HEK293T, NoDiceΔPKR:ctrl and FHA:DICER
1211 mutant cell lines infected with SINV-GFP at an MOI of 0.02 for 24h. The left panel corresponds
1212 to GFP signal from infected cells and the right panel to a merge picture of GFP signal and
1213 brightfield. Pictures were taken with 5x magnification. hpi: hours post-infection. **B.** Western
1214 blot analysis of DICER (DICER and HA), AGO2, PKR and GFP expression in SINV-GFP-
1215 infected HEK293T, NoDiceΔPKR FHA:ctrl and FHA:DICER mutant cell lines shown in **A.**
1216 Gamma-Tubulin was used as loading control. **C.** Mean (+/-SEM) of SINV-GFP viral titers in
1217 the same cell lines as in **A.** infected at an MOI of 0.02 for 24h (n = 3) from plaque assay
1218 quantification. ns: non-significant, ordinary one-way ANOVA test with Bonferroni correction.
1219

1220 # Supplementary material

1221 ## Supplementary figure legends

1222 **Figure S1. Analysis of SINV-GFP infection in FHA:DICER cell lines at different MOI**
1223 **and time points.**

1224 **A.** miR-16 expression analyzed by northern blot in HEK293T, NoDice FHA:ctrl #1 and
1225 FHA:DICER WT #4 cell lines**.** Expression of snRNA U6 was used as loading control. **B.**
1226 Representative GFP pictures of HEK293T, NoDice 2.20, NoDice 4.25, NoDice FHA:ctrl #1
1227 and NoDice FHA:ctrl #2 cells infected with SINV-GFP at an MOI of 0.02 for 24h. The left
1228 panel corresponds to GFP signal and the right panel to a merge of GFP signal and the
1229 corresponding brightfield. Pictures were taken with a 5x magnification. hpi: hours post-
1230 infection. **C.** Mean (+/- SEM) of SINV-GFP viral titers in cells infected at an MOI of 0.02 for
1231 24 h (n=3) from plaque assay quantification. * $p < 0.05$, ns: non-significant, ordinary one-way
1232 ANOVA test with Bonferroni correction. **D**. Western blot analysis of DICER, AGO2 and GFP
1233 expression in SINV-GFP-infected cells shown in B. Gamma-Tubulin was used as loading
1234 control.

1235

1236 **Figure S2. LC-MS/MS analysis of DICER interactome during SFV infection.**

1237 **A.** Volcano plot for differentially expressed proteins (DEPs) between HA IP and CTL IP in
1238 FHA:DICER mock-infected cells. Each protein is marked as a dot; proteins that are
1239 significantly up-regulated in HA IP are shown in red, up-regulated proteins in CTL IP are
1240 shown in blue, and non-significant proteins are in black. The horizontal line denotes a p-value
1241 of 0.05 and the vertical lines the Log2 fold change cutoff (-1 and 1). DICER and its cofactors
1242 (TRBP, PACT, AGO2) are highlighted in yellow. **B.** Left panel: Volcano plot for DEPs
1243 between SFV (MOI of 2, 6 hpi) and mock fractions of HA IP in FHA:DICER cells. Same colour
1244 code and thresholds as in A were applied. Proteins that are discussed in the text are highlighted
1245 in yellow and SFV proteins in purple. **C.** Summary of the differential expression analysis of
1246 SFV vs mock fractions from HA IP in FHA:DICER cells. The analysis has been performed
1247 using a generalized linear model of a negative-binomial distribution and p-values were
1248 corrected for multiple testing using the Benjamini-Hochberg method.

1249

1250 **Figure S3. Confirmation of LC-MS/MS analysis by co-IP and BiFC controls.**

1251 **A.** FHA:DICER WT #4 cells were infected with SINV-GFP at an MOI of 0.02 for 24 h and a
1252 HA co-IP was performed. Eluted proteins were resolved by western blot and IP efficiency was

1253 assessed using an HA antibody. In parallel, co-IPed proteins were visualized using appropriate
1254 antibodies. GFP antibody was used to verify the infection and Ponceau staining serves as
1255 loading control. **B.** 1% Agarose gel analysis of RNA extracted from INPUT of the co-IP in Fig.
1256 3B. Ribosomal RNA integrity was compared to a control HEK293T cell line. RNAs were
1257 revealed using ethidium bromide under UV. **C.** Schematic representation of Human DICER
1258 proteins used for BiFC positive and negative controls. The different conserved domains are
1259 shown in colored boxes. DUF283: Domain of Unknown Function; PAZ: PIWI ARGONAUTE
1260 ZWILLE domain; dsRBD: dsRNA-binding domain. hDICER WT is the full-length protein.
1261 hDICER N1 is deleted of the first N-terminal 495 amino acids. **D.** Expression of BiFC plasmids
1262 was assessed by western blot. DICER proteins (WT and N1) and PKR were visualized using
1263 antibodies targeting endogenous proteins, whereas TRBP and PACT were detected using GFP
1264 antibody. Antibody targeting the SINV coat protein (CP) was used as infection control. Ponceau
1265 staining was used as loading control. **E.** Positive and negative BiFC controls on fixed
1266 NoDice/ΔPKR cells. After co-transfection, cells were infected with SINV at an MOI of 2 for 6
1267 h and fixed. After fixation, cells were stained with DAPI and observed under confocal
1268 microscope. Merge pictures of BiFC and DAPI signals of SINV-infected cells are shown. A
1269 higher magnification of images showing the interaction represented by a red square is shown
1270 in the bottom left corner. Scale bar: 20 µm and 10 µm. **F.** Expression of BiFC plasmids was
1271 assessed by western blot. DICER, PKR, TRBP and PACT were detected using GFP antibody.
1272 Antibody targeting the SINV coat protein (CP) was used as infection control. Gamma-Tubulin
1273 was used as loading control. The asterisk corresponds to an aspecific band. **G.** Interactions
1274 between DICER and TRBP, PACT or PKR were visualized by BiFC. Plasmids expressing $^{N-}$
1275 ^{ter}Venus:DICER and TRBP:, PACT: or PKR:Venus^{C-ter} were co-transfected in HEK293T cells
1276 for 24 h and cells were either infected with SINV at an MOI of 2 for 6 h or not. The different
1277 combinations are indicated on the left side. Reconstitution of Venus (BiFC) signal was observed
1278 under epifluorescence microscope. For each condition, the left panel corresponds to Venus
1279 signal and the right panel to the corresponding brightfield pictures. Scale bar: 100 µm.
1280

1281 **Figure S4. Confirmation of DICER interactome upon SINV infection in HCT116 KI-**
1282 **DICER cells.**

1283 **A.** Schematic representation of DICER WT and Flag-HA(FHA)-GFP kocked-in (KI) alleles.
1284 FHA sequence is in purple, GFP in green, DICER 5'UTR in orange and DICER coding region
1285 in yellow. The gRNA used to generate the KI was designed to target the first coding exon of

1286 DICER gene. **B.** PCR on genomic DNA extracted from WT and KI cells. **C.** An oligo outside
1287 the homologous recombination region and an oligo within the GFP tag were used to verify the
1288 presence of a 1040bp amplicon in HCT116 KI-DICER clone. Sequencing results corresponding
1289 to this region are shown. **D.** Western blot analysis of DICER, p-PKR, PKR and p-eIF2α
1290 expression in mock or SINVGFP-infected HEK293T and HCT116 KI-DICER cell lines at an
1291 MOI of 2 for 6h or 16h and 0.02 for 24h. GFP antibody was used to verify the infection. Ponceau
1292 and gamma-Tubulin were used as loading control.
1293
1294 **Figure S5. Interaction analysis between the different versions of DICER and TRBP or**
1295 **PACT using BiFC assay.**
1296 NoDice/ΔPKR cells were co-transfected for 24 h with plasmids expressing the different
1297 versions of DICER proteins fused to the N-terminal part of Venus and either TRBP:Venus$^{C\text{-}ter}$
1298 (**A**) or PACT:Venus$^{C\text{-}ter}$ (**B**). Cells were then infected with SINV at an MOI of 2 for 6 h and
1299 Venus signal was observed under epifluorescence microscope. The left panel corresponds to
1300 Venus signal and the right panel to the corresponding brightfield picture. Pictures were taken
1301 with a 5x magnification. hpi: hours post-infection. Scale bar: 100 μm.
1302
1303 **Figure S6. Analysis of the importance of Dicer helicase domain on SINV-GFP infection in**
1304 **FHA:DICER mutant stable cell lines.**
1305 **A**. Northern blot analysis of miR-16 expression in HEK293T, NoDice 2.20, NoDice FHA:ctrl
1306 #2, FHA:DICER WT polyclonal, FHA:DICER N1 #6, FHA:DICER Hel. #2.6, and
1307 FHA:DICER N3 #2.13. Expression of snRNA U6 was used as loading control. **B.**
1308 Representative GFP fluorescent microscopy images of HEK293T, NoDice 2.20, FHA:DICER
1309 mutants cell lines infected with SINV-GFP at an MOI of 0.02 for 24 h. The left panel
1310 corresponds to GFP signal and the right panel to a merge picture of GFP signal and brightfield.
1311 Pictures were taken with a 5x magnification. hpi: hours post-infection. **C**. Mean (+/- SEM) of
1312 SINV-GFP viral titers over FHA:DICER WT #4 cells in FHA:DICER N1 #6, FHA:DICER N3
1313 #2.13, NoDice FHA:ctrl #2 and NoDice 2.20 cell lines infected at an MOI of 0.02 for 24 h (n
1314 = 3) from plaque assay quantification. *** $p < 0.001$, ns: non-significant, ordinary one-way
1315 ANOVA test with Bonferroni correction.
1316
1317
1318

1319 **Supplementary tables**

1320 **Supp. Table 1:** Top 100 proteins that are differentially immunoprecipitated in mock-infected
1321 FHA:DICER cells by the HA and Myc (CTL) antibodies. Related to Figure 2.

1322

1323 **Supp. Table 2:** Top 100 proteins that are differentially immunoprecipitated with the HA
1324 antibody in SINV-infected vs mock-infected FHA:DICER cells. Related to Figure 2.

1325

1326 **Supp. Table 3:** Top 100 proteins that are differentially immunoprecipitated in mock-infected
1327 FHA:DICER cells by the HA and Myc (CTL) antibodies, in the SFV infection experiment.
1328 Related to Figure S2.

1329

1330 **Supp. Table 4:** Top 100 proteins that are differentially immunoprecipitated with the HA
1331 antibody in SFV-infected vs mock-infected FHA:DICER cells. Related to Figure S2.

1332

1333 **Supp. Table 5:** List of primers used in this study.

1334

1335 **Supp. Table 6:** data and statistical tests details used in plaque assays shown in Figures 1, 6, 7,
1336 8, S1 and S6

Figure 1

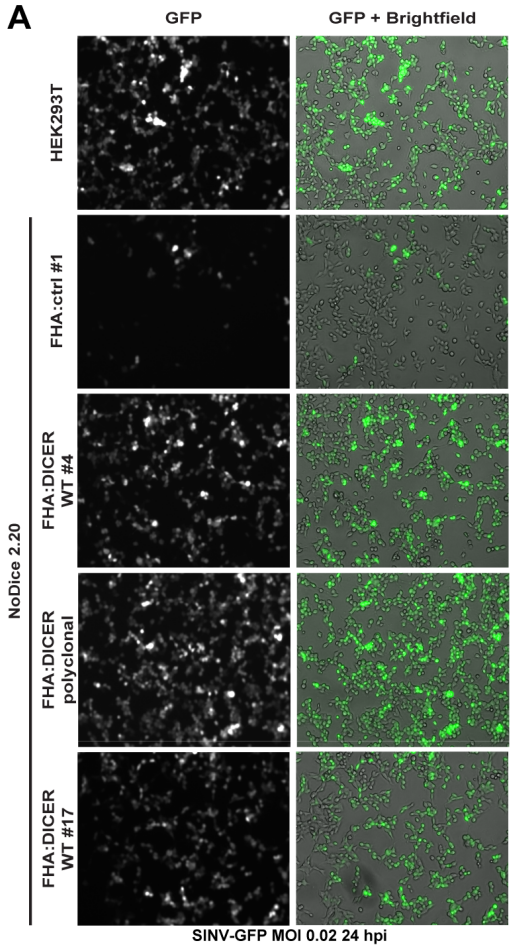
A
GFP
GFP + Brightfield
HEK293T
FHA:ctrl #1
FHA:DICER WT #4
FHA:DICER polyclonal
FHA:DICER WT #17
NoDice 2.20
SINV-GFP MOI 0.02 24 hpi

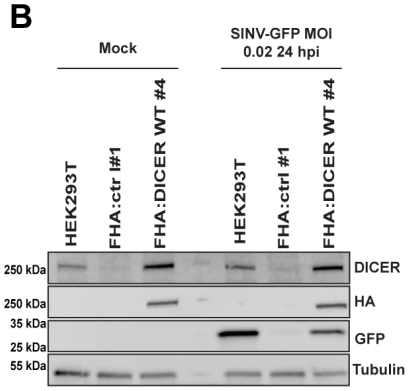
B
Mock
SINV-GFP MOI 0.02 24 hpi
HEK293T
FHA:ctr l#1
FHA:DICER WT #4
HEK293T
FHA:ctrl #1
FHA:DICER WT #4
250 kDa
DICER
250 kDa
HA
35 kDa
25 kDa
GFP
55 kDa
Tubulin

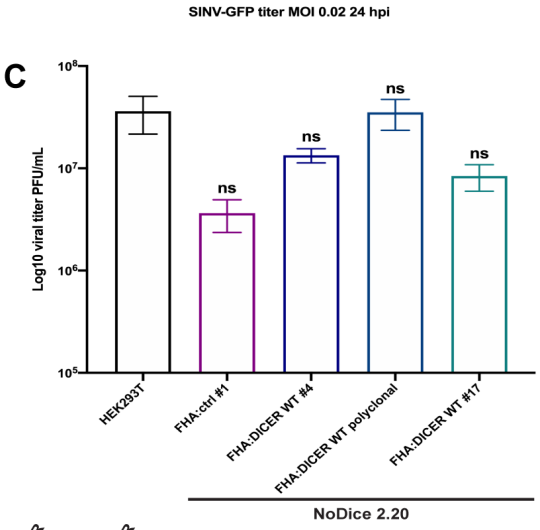
SINV-GFP titer MOI 0.02 24 hpi
C
Log10 viral titer PFU/mL
10^8
10^7
10^6
10^5
ns
ns
ns
ns
HEK293T
FHA:ctrl #1
FHA:DICER WT #4
FHA:DICER WT polyclonal
FHA:DICER WT #17
NoDice 2.20

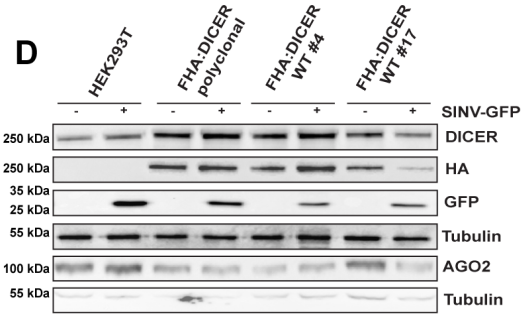
D
HEK293T
FHA:DICER polyclonal
FHA:DICER WT #4
FHA:DICER WT #17
SINV-GFP
- + - + - + - +
250 kDa
DICER
250 kDa
HA
35 kDa
25 kDa
GFP
55 kDa
Tubulin
100 kDa
AGO2
55 kDa
Tubulin

Figure 2

A

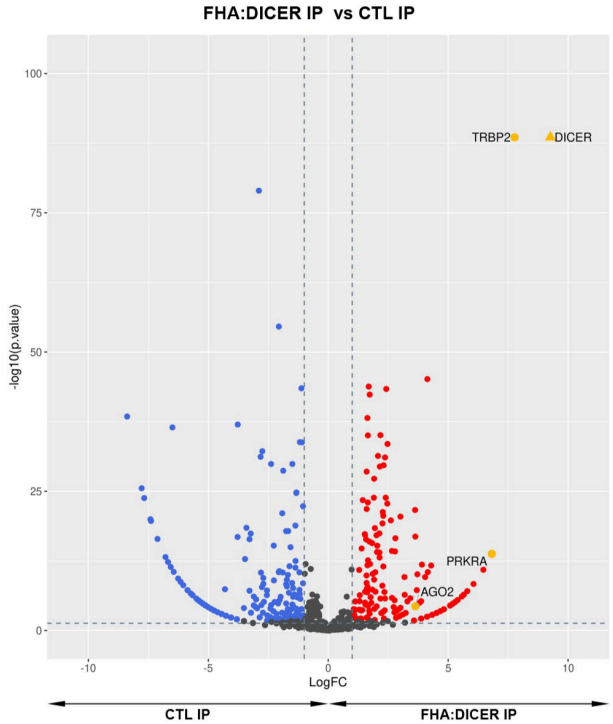

B

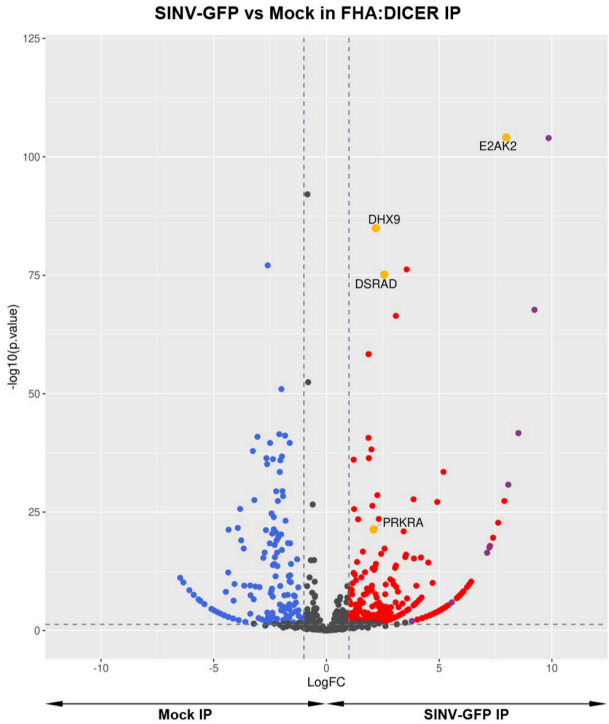

C

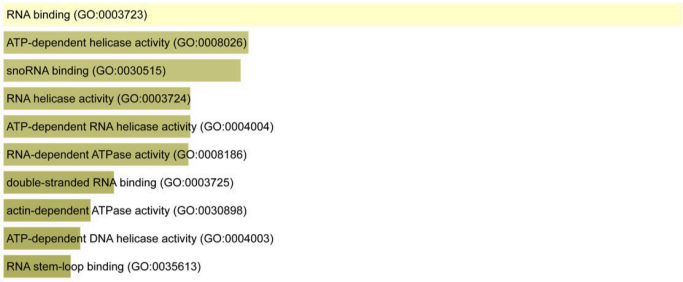

D

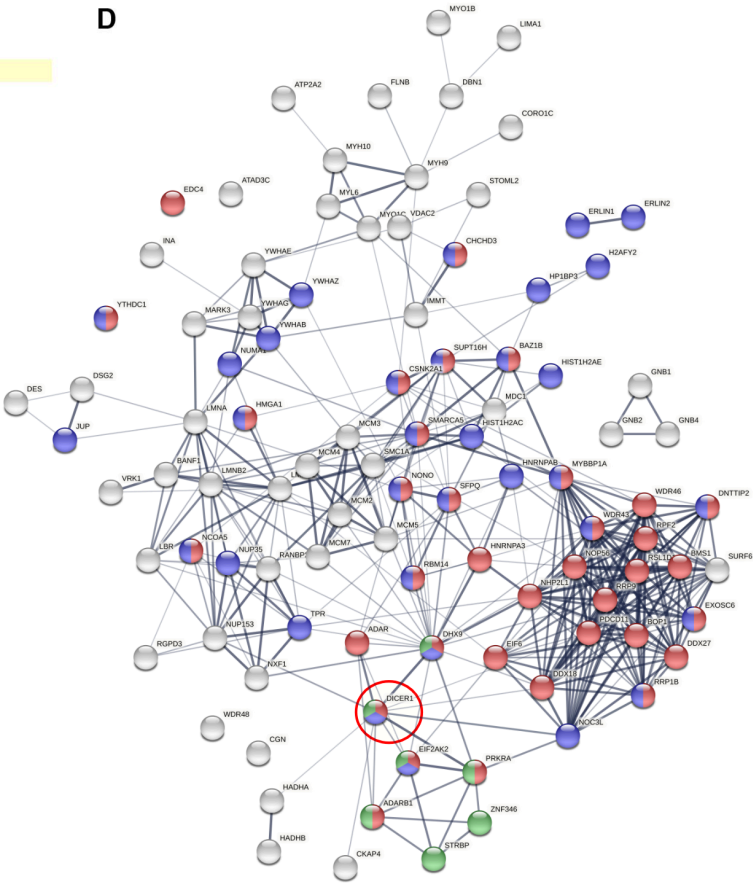
DICER1
EIF2AK2
PRKRA
ADAR
DHX9
ADARB1
ZNF346
STRBP
CKAP4
HADHA
HADHB
CGN
WDR48
NOC3L
TPR
NUP153
RGPD3
NXF1
EIF6
DDX27
RRP1B
EXOSC6
SURF6
DNTTIP2
WDR46
HNRNPA3
RBM14
NONO
SFPQ
HNRNPAB
MYBBP1A
SMARCA5
HIST1H2AC
CSNK2A1
SUPT16H
BAZ1B
HIST1H2AE
GNB1
GNB2
GNB4
ERLIN1
ERLIN2
H2AFY2
HP1BP3
CHCHD3
IMMT
VDAC2
STOML2
MYO1C
MYL6
MYH9
MYH10
ATP2A2
FLNB
DBN1
CORO1C
MYO1B
LIMA1
EDC4
ATAD3C
INA
YWHAE
YWHAZ
YWHAG
YWHAB
YTHDC1
MARK3
NUMA1
MDC1
HMGA1
LMNA
DES
DSG2
JUP
BANF1
LMNB2
VRK1
MCM3
MCM4
MCM2
MCM5
MCM7
SMC1A
RANBP2
NUP35
NCOA5
LBR
NHP2L1
RRP9
BOP1
PES1
BMS1
RSL1D1
NOP56
NOP58
RPF2
WDR43
WDR46
DDX18
DDX21
DDX10
DDX51
DDX52
DDX54
DDX56
DDX47
DDX49

Figure 3

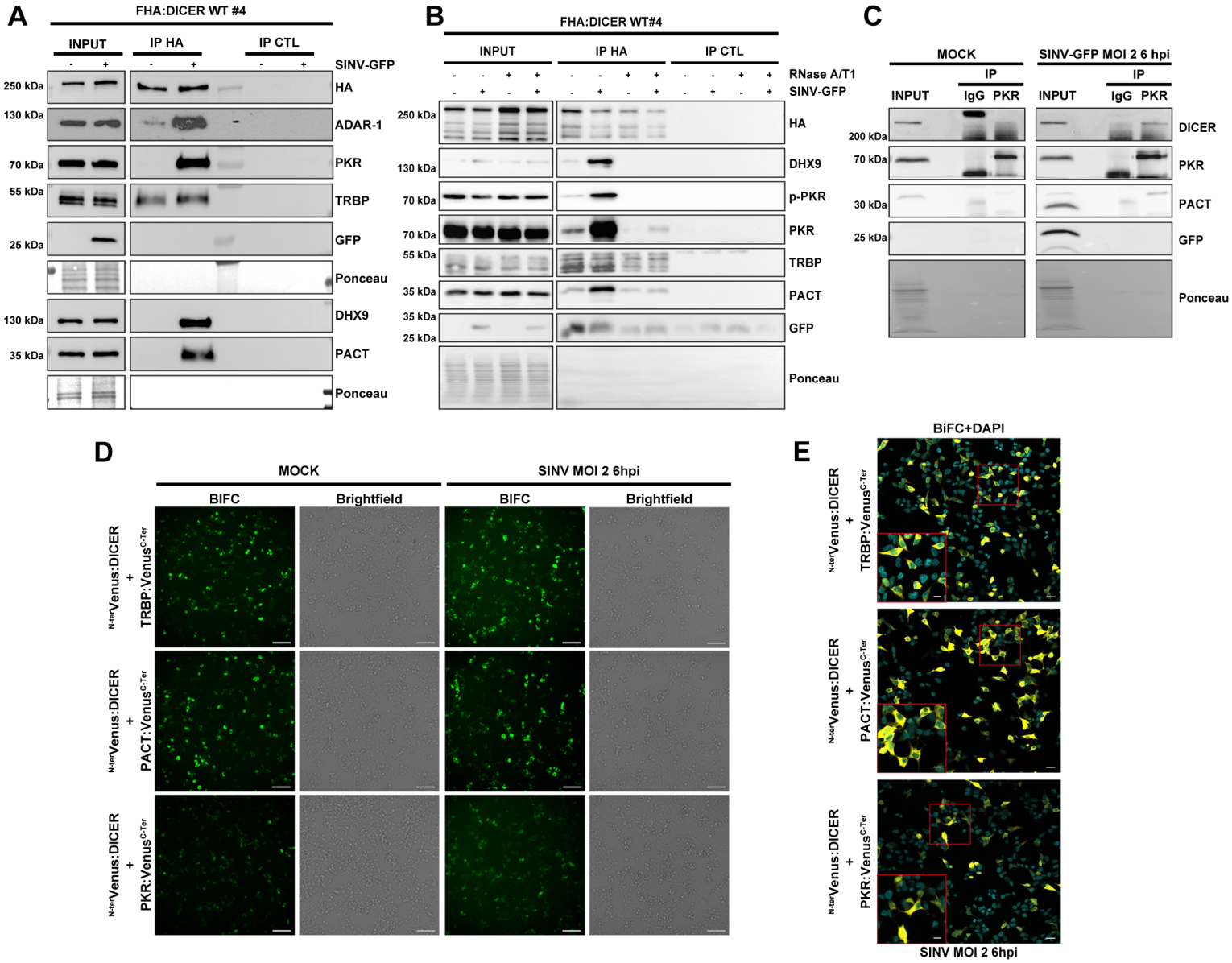
A
FHA:DICER WT #4
INPUT
IP HA
IP CTL
SINV-GFP
250 kDa
HA
130 kDa
ADAR-1
70 kDa
PKR
55 kDa
TRBP
25 kDa
GFP
Ponceau
130 kDa
DHX9
35 kDa
PACT
Ponceau
B
FHA:DICER WT#4
INPUT
IP HA
IP CTL
RNase A/T1
SINV-GFP
250 kDa
HA
130 kDa
DHX9
70 kDa
p-PKR
70 kDa
PKR
55 kDa
TRBP
35 kDa
PACT
35 kDa
25 kDa
GFP
Ponceau
C
MOCK
SINV-GFP MOI 2 6 hpi
IP
INPUT
IgG
PKR
200 kDa
DICER
70 kDa
PKR
30 kDa
PACT
25 kDa
GFP
Ponceau
D
MOCK
SINV MOI 2 6hpi
BIFC
Brightfield
N-terVenus:DICER + TRBP:VenusC-Ter
N-terVenus:DICER + PACT:VenusC-Ter
N-terVenus:DICER + PKR:VenusC-Ter
E
BiFC+DAPI
N-terVenus:DICER + TRBP:VenusC-Ter
N-terVenus:DICER + PACT:VenusC-Ter
N-terVenus:DICER + PKR:VenusC-Ter
SINV MOI 2 6hpi

Figure 4

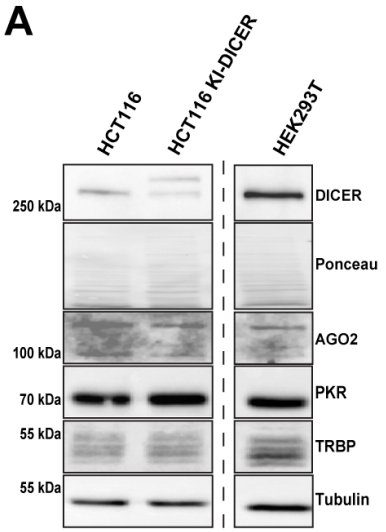
A
HCT116
HCT116 KI-DICER
HEK293T
250 kDa
DICER
Ponceau
100 kDa
AGO2
70 kDa
PKR
55 kDa
TRBP
55 kDa
Tubulin

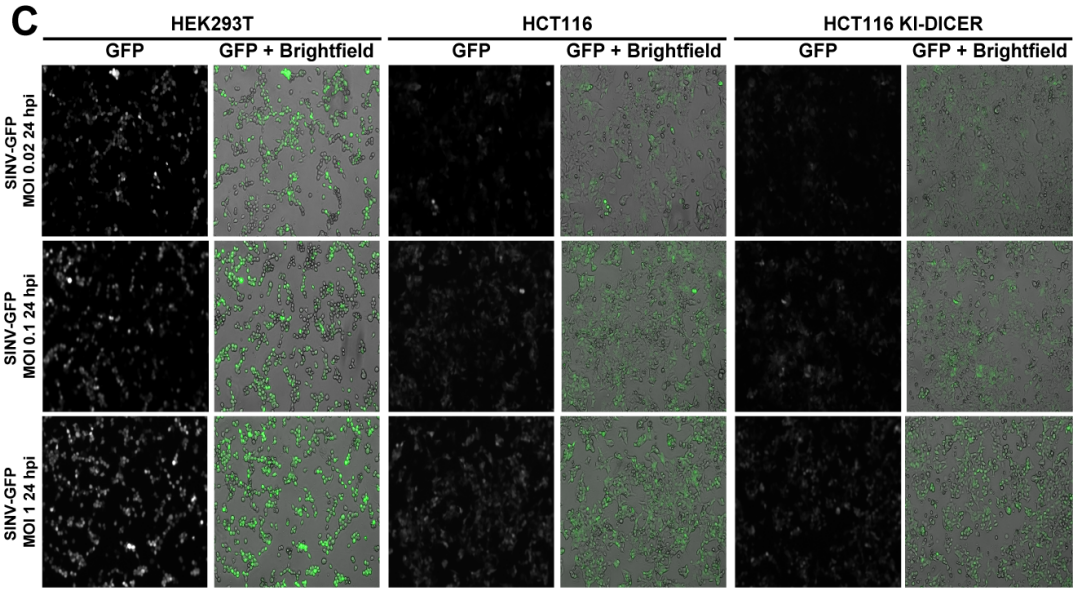
C
HEK293T
HCT116
HCT116 KI-DICER
GFP
GFP + Brightfield
SINV-GFP MOI 0.02 24 hpi
SINV-GFP MOI 0.1 24 hpi
SINV-GFP MOI 1 24 hpi

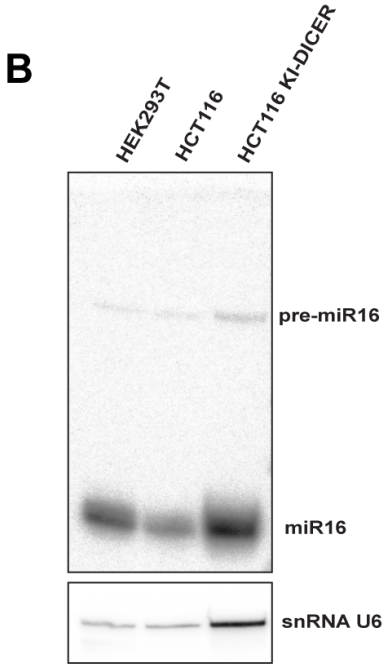
B
HEK293T
HCT116
HCT116 KI-DICER
pre-miR16
miR16
snRNA U6

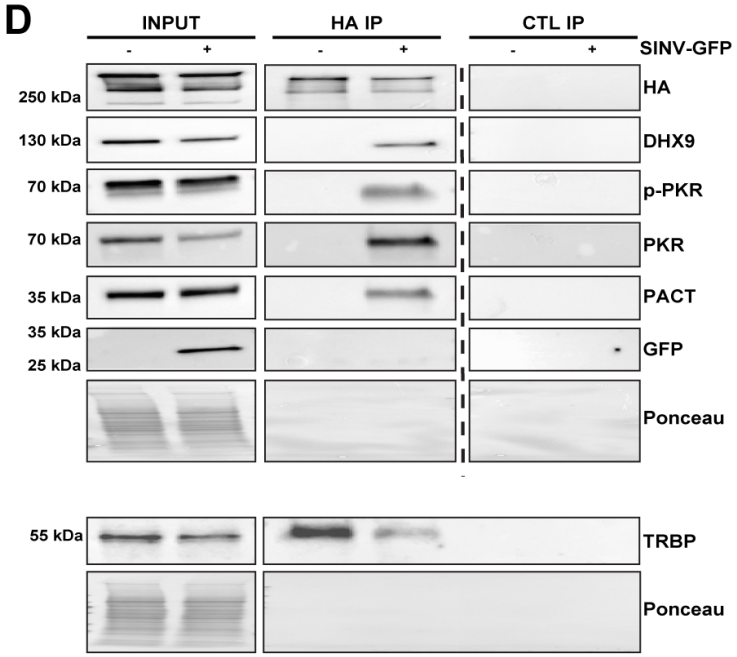
D
INPUT
HA IP
CTL IP
-
+
SINV-GFP
250 kDa
HA
130 kDa
DHX9
70 kDa
p-PKR
70 kDa
PKR
35 kDa
PACT
35 kDa
25 kDa
GFP
Ponceau
55 kDa
TRBP
Ponceau

Figure 5

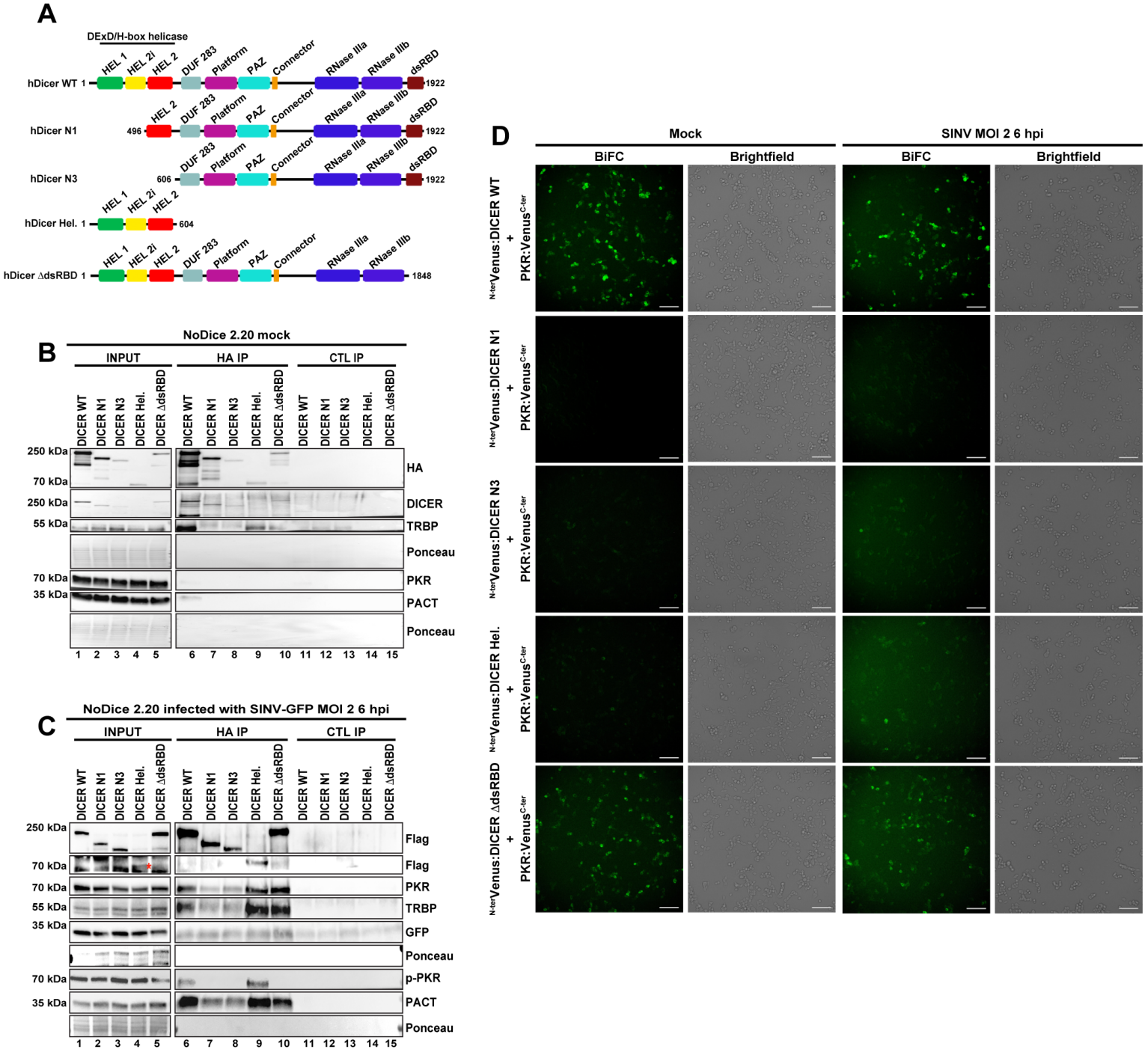
A
DExD/H-box helicase
HEL 1
HEL 2i
HEL 2
DUF 283
Platform
PAZ
Connector
RNase IIIa
RNase IIIb
dsRBD
hDicer WT 1
1922
hDicer N1
496
hDicer N3
606
hDicer Hel. 1
604
hDicer ΔdsRBD 1
1848
B
NoDice 2.20 mock
INPUT
HA IP
CTL IP
DICER WT
DICER N1
DICER N3
DICER Hel.
DICER ΔdsRBD
250 kDa
70 kDa
55 kDa
35 kDa
HA
DICER
TRBP
Ponceau
PKR
PACT
1 2 3 4 5 6 7 8 9 10 11 12 13 14 15
C
NoDice 2.20 infected with SINV-GFP MOI 2 6 hpi
Flag
p-PKR
GFP
D
Mock
SINV MOI 2 6 hpi
BiFC
Brightfield
N-terVenus:DICER WT
N-terVenus:DICER N1
N-terVenus:DICER N3
N-terVenus:DICER Hel.
N-terVenus:DICER ΔdsRBD
+
PKR:VenusC-ter

Figure 6

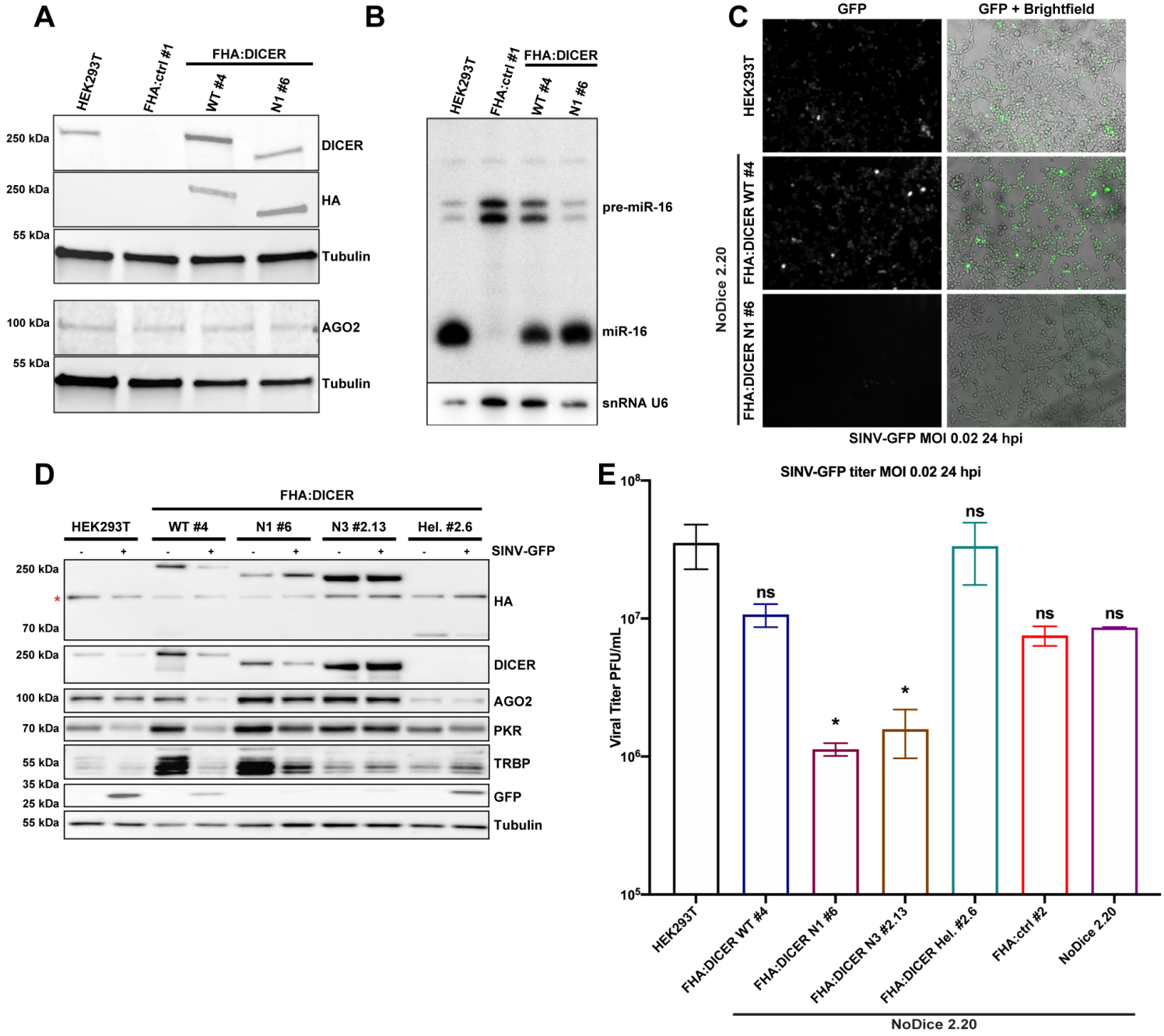
A
HEK293T
FHA:ctrl #1
FHA:DICER
WT #4
N1 #6
250 kDa
DICER
250 kDa
HA
55 kDa
Tubulin
100 kDa
AGO2
55 kDa
Tubulin
B
HEK293T
FHA:ctrl #1
FHA:DICER
WT #4
N1 #6
pre-miR-16
miR-16
snRNA U6
C
GFP
GFP + Brightfield
HEK293T
NoDice 2.20
FHA:DICER WT #4
FHA:DICER N1 #6
SINV-GFP MOI 0.02 24 hpi
D
FHA:DICER
HEK293T
WT #4
N1 #6
N3 #2.13
Hel. #2.6
SINV-GFP
250 kDa
HA
70 kDa
250 kDa
DICER
100 kDa
AGO2
70 kDa
PKR
55 kDa
TRBP
35 kDa
25 kDa
GFP
55 kDa
Tubulin
E
SINV-GFP titer MOI 0.02 24 hpi
Viral Titer PFU/mL
ns
*
HEK293T
FHA:DICER WT #4
FHA:DICER N1 #6
FHA:DICER N3 #2.13
FHA:DICER Hel. #2.6
FHA:ctrl #2
NoDice 2.20
NoDice 2.20

Figure 7

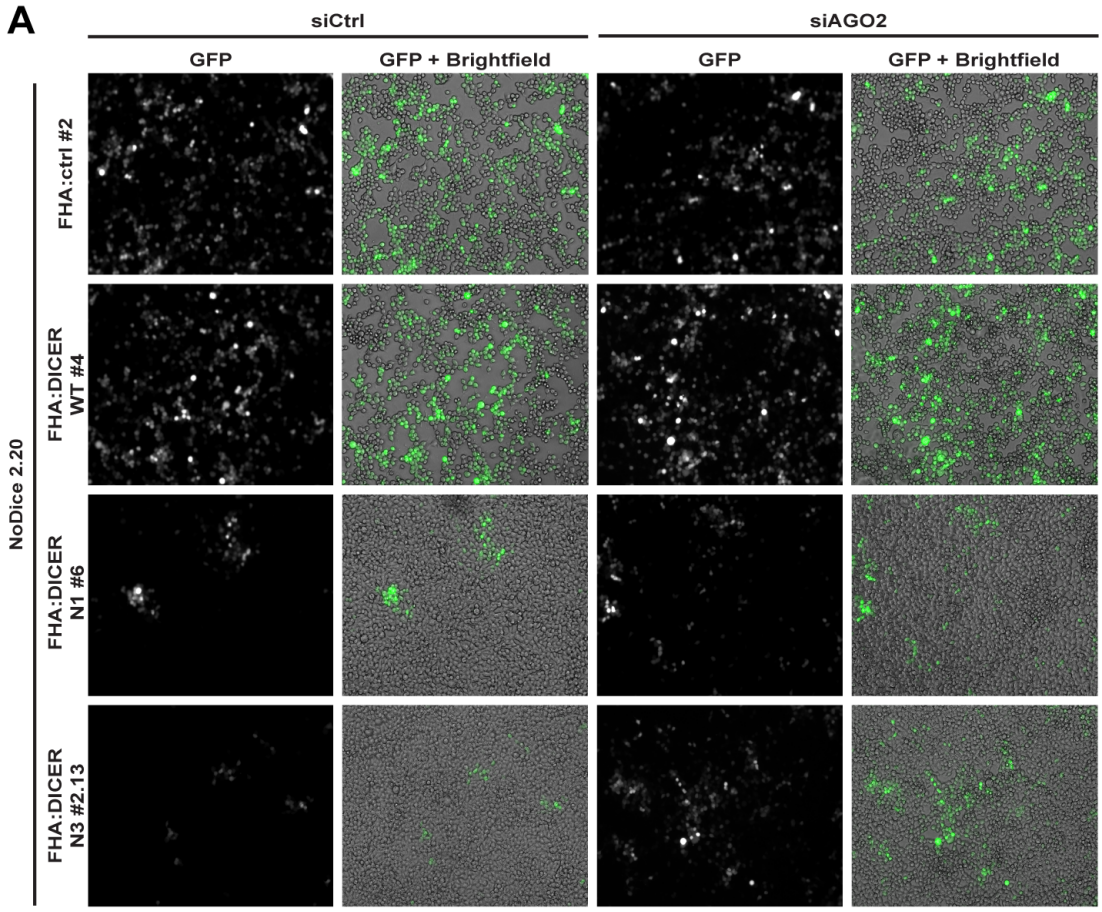
A
siCtrl
siAGO2
GFP
GFP + Brightfield
GFP
GFP + Brightfield
NoDice 2.20
FHA:ctrl #2
FHA:DICER WT #4
FHA:DICER N1 #6
FHA:DICER N3 #2.13
SINV-GFP MOI 0.02 24hpi

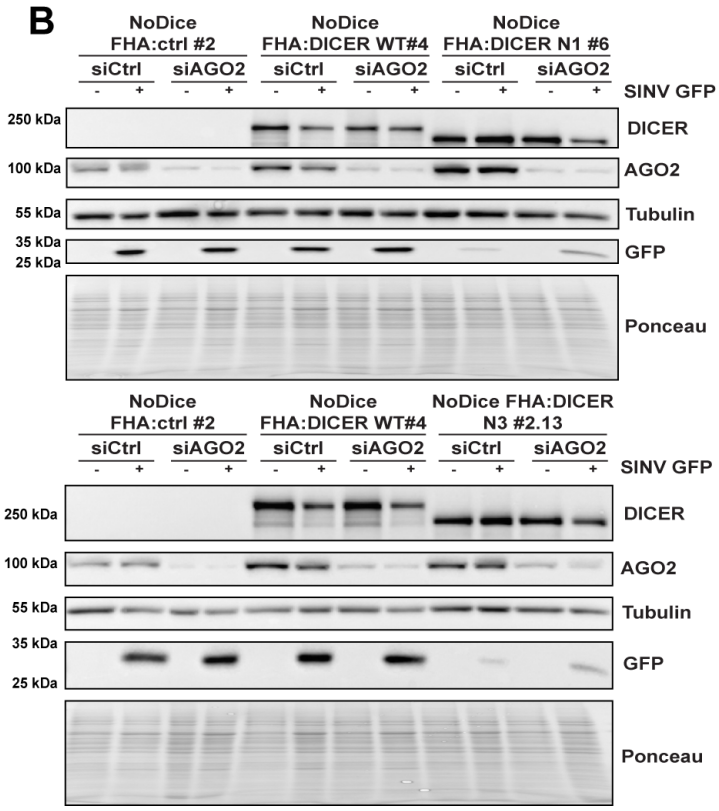
B
NoDice FHA:ctrl #2
NoDice FHA:DICER WT#4
NoDice FHA:DICER N1 #6
siCtrl
siAGO2
SINV GFP
250 kDa
100 kDa
55 kDa
35 kDa
25 kDa
DICER
AGO2
Tubulin
GFP
Ponceau
NoDice FHA:DICER N3 #2.13

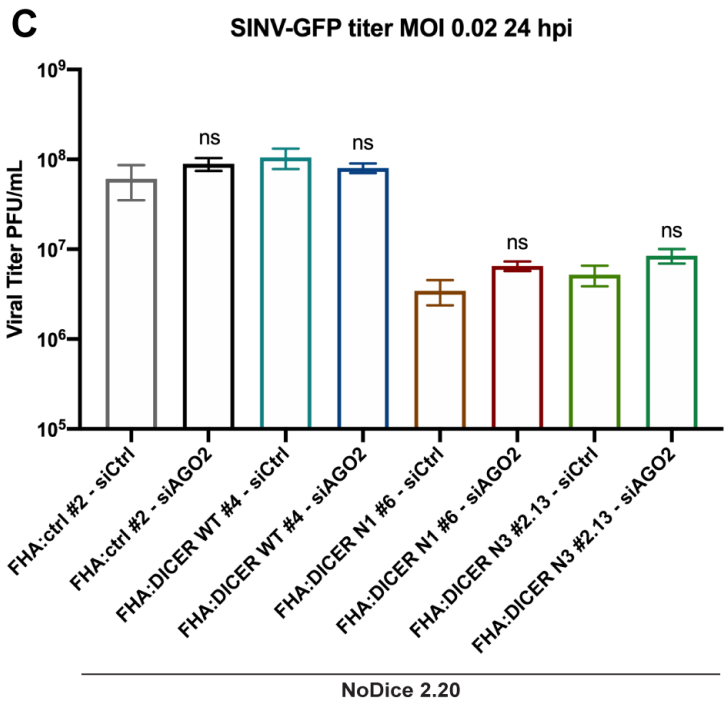
C
SINV-GFP titer MOI 0.02 24 hpi
Viral Titer PFU/mL
ns
FHA:ctrl #2 - siCtrl
FHA:ctrl #2 - siAGO2
FHA:DICER WT #4 - siCtrl
FHA:DICER WT #4 - siAGO2
FHA:DICER N1 #6 - siCtrl
FHA:DICER N1 #6 - siAGO2
FHA:DICER N3 #2.13 - siCtrl
FHA:DICER N3 #2.13 - siAGO2
NoDice 2.20

Figure 8

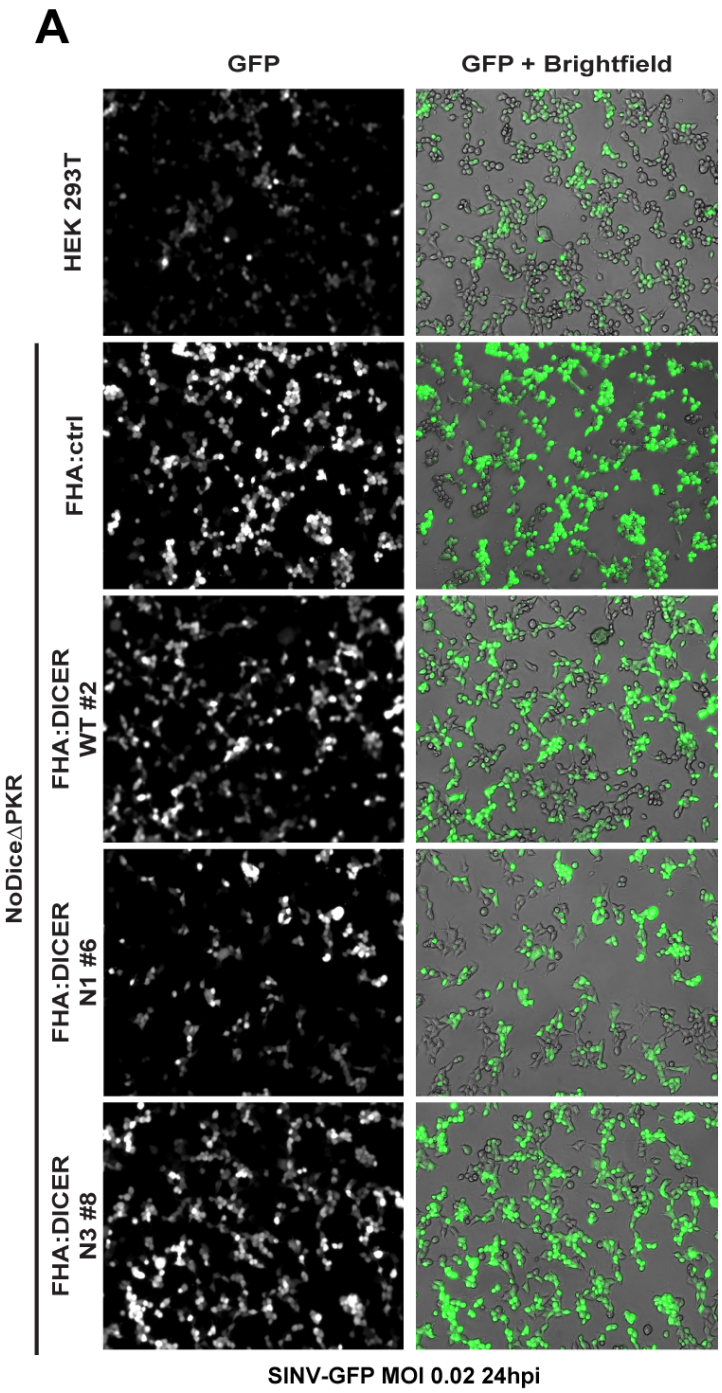
A
GFP
GFP + Brightfield
HEK 293T
FHA:ctrl
FHA:DICER WT #2
FHA:DICER N1 #6
FHA:DICER N3 #8
NoDiceΔPKR
SINV-GFP MOI 0.02 24hpi

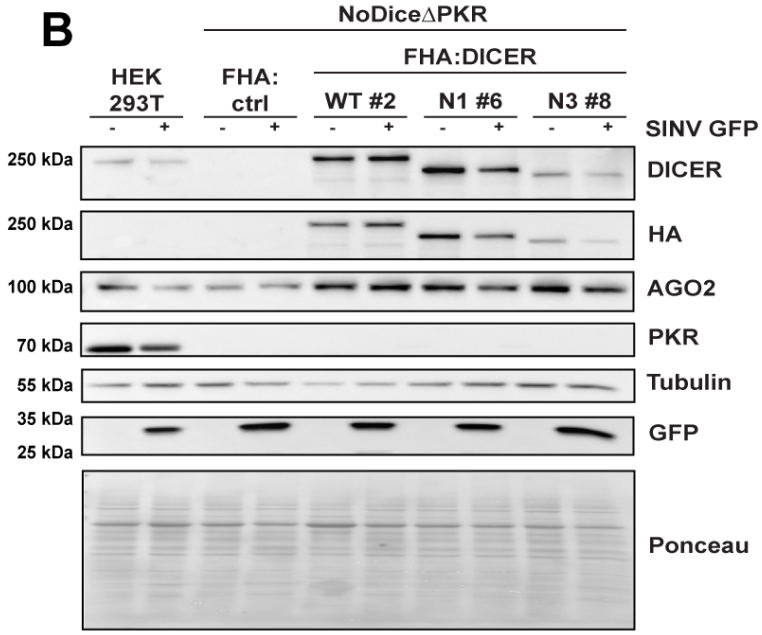
B
NoDiceΔPKR
FHA:DICER
HEK 293T
FHA: ctrl
WT #2
N1 #6
N3 #8
- + - + - + - + - +
SINV GFP
250 kDa
DICER
250 kDa
HA
100 kDa
AGO2
70 kDa
PKR
55 kDa
Tubulin
35 kDa
25 kDa
GFP
Ponceau

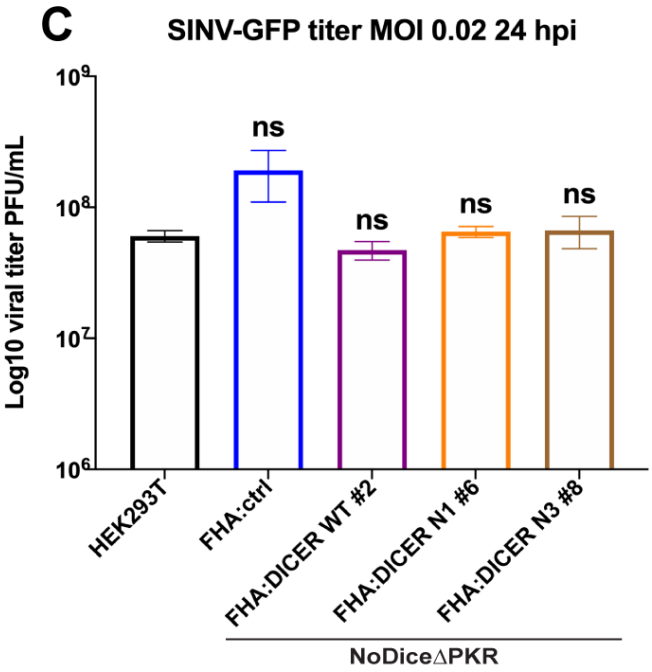
C
SINV-GFP titer MOI 0.02 24 hpi
Log10 viral titer PFU/mL
10^9
10^8
10^7
10^6
ns
ns
ns
ns
HEK293T
FHA:ctrl
FHA:DICER WT #2
FHA:DICER N1 #6
FHA:DICER N3 #8
NoDiceΔPKR